Deep-Sea Research II 127 (2016) 7–27

Contents lists available at ScienceDirect

Deep-Sea Research II

journal homepage: www.elsevier.com/locate/dsr2

Physical and biogeochemical controls on the variability in surface pH and calcium carbonate saturation states in the Atlantic sectors of the Arctic and Southern Oceans

Eithne Tynan [a,*], Jennifer S. Clarke [a], Matthew P. Humphreys [a], Mariana Ribas-Ribas [a,b], Mario Esposito [a], Victoire M.C. Rérolle [a,c], C. Schlosser [a,d], Sally E. Thorpe [e], Toby Tyrrell [a], Eric P. Achterberg [a,d]

[a] Ocean and Earth Science, University of Southampton, National Oceanography Centre Southampton, Southampton SO14 3ZH, United Kingdom
[b] Carl von Ossietzky Universität Oldenburg, Institute for Chemistry and Biology of the Marine Environment, 26382 Wilhelmshaven, Germany
[c] Sorbonne Universités (UPMC, Univ Paris 06)-CNRS-IRD-MNHN, LOCEAN Laboratory, 75005, France
[d] GEOMAR Helmholtz Centre for Ocean Research Kiel, 24148 Kiel, Germany
[e] British Antarctic Survey, Natural Environment Research Council, High Cross, Madingley Road, Cambridge CB3 0ET, United Kingdom

ARTICLE INFO

Available online 29 January 2016

Keywords:
Carbonate system
Ocean acidification
Arctic Ocean
Southern Ocean
Biogeochemistry

ABSTRACT

Polar oceans are particularly vulnerable to ocean acidification due to their low temperatures and reduced buffering capacity, and are expected to experience extensive low pH conditions and reduced carbonate mineral saturations states (Ω) in the near future. However, the impact of anthropogenic CO_2 on pH and Ω will vary regionally between and across the Arctic and Southern Oceans. Here we investigate the carbonate chemistry in the Atlantic sector of two polar oceans, the Nordic Seas and Barents Sea in the Arctic Ocean, and the Scotia and Weddell Seas in the Southern Ocean, to determine the physical and biogeochemical processes that control surface pH and Ω. High-resolution observations showed large gradients in surface pH (0.10–0.30) and aragonite saturation state (Ω_{ar}) (0.2–1.0) over small spatial scales, and these were particularly strong in sea-ice covered areas (up to 0.45 in pH and 2.0 in Ω_{ar}). In the Arctic, sea-ice melt facilitated bloom initiation in light-limited and iron replete (dFe > 0.2 nM) regions, such as the Fram Strait, resulting in high pH (8.45) and Ω_{ar} (3.0) along the sea-ice edge. In contrast, accumulation of dissolved inorganic carbon derived from organic carbon mineralisation under the ice resulted in low pH (8.05) and Ω_{ar} (1.1) in areas where thick ice persisted. In the Southern Ocean, sea-ice retreat resulted in bloom formation only where terrestrial inputs supplied sufficient iron (dFe > 0.2 nM), such as in the vicinity of the South Sandwich Islands where enhanced pH (8.3) and Ω_{ar} (2.3) were primarily due to biological production. In contrast, in the adjacent Weddell Sea, weak biological uptake of CO_2 due to low iron concentrations (dFe < 0.2 nM) resulted in low pH (8.1) and Ω_{ar} (1.6). The large spatial variability in both polar oceans highlights the need for spatially resolved surface data of carbonate chemistry variables but also nutrients (including iron) in order to accurately elucidate the large gradients experienced by marine organisms and to understand their response to increased CO_2 in the future.

1. Introduction

Polar regions are particularly sensitive to rising temperatures and increasing atmospheric CO_2 concentrations (Stocker et al., 2013). Arctic sea-ice has decreased in summer extent (Comiso, 2011; Stroeve et al., 2012) and thickness (Kwok and Cunningham, 2010) over the last few decades, and observed warming in this region is currently almost twice that in the Northern Hemisphere as a whole (Serreze et al., 2009). In contrast, Antarctic sea-ice extent has remained steady or even increased (Maksym et al., 2012), and warming follows the general global trend (Turner and Overland, 2009), but strong regional differences exist. In particular, the Western Antarctic Peninsula experiences higher rates of warming (Vaughan et al., 2003) with decreasing sea-ice (Stammerjohn et al., 2008) and retreating ice shelves (Wouters et al., 2015). Ocean acidification in polar regions adds pressure to already stressed ecosystems (Stocker et al., 2013; Orr et al., 2005).

The uptake of CO_2 by the oceans alters the chemistry of seawater and increases dissolved inorganic carbon (DIC) and bicarbonate ion concentrations, and reduces carbonate ion

* Corresponding author.
E-mail address: eithne.tynan@gmail.com (E. Tynan).

http://dx.doi.org/10.1016/j.dsr2.2016.01.001

concentrations, calcium carbonate mineral saturation states (Ω) and pH (Caldeira and Wickett, 2003; Cao et al., 2007; Zeebe and Wolf-Gladrow, 2001). High-latitude oceans have naturally lower pH, Ω and buffering capacity (Sabine et al., 2004) due to a higher solubility of CO_2 in their cold waters, and are expected to be the first to experience undersaturation ($\Omega < 1$) for calcium carbonate minerals (McNeil and Matear, 2008; Steinacher et al., 2009). In fact, surface waters of the Arctic Ocean already experience seasonal undersaturation due to increased sea-ice melt (Robbins et al., 2013; Yamamoto-Kawai et al., 2009), river runoff (Azetsu-Scott et al., 2014; Chierici and Fransson, 2009) and Pacific water intrusion (Azetsu-Scott et al., 2010).

Undersaturated waters can be corrosive to calcifying organisms which lack protective mechanisms and/or rely on seawater pH for calcification (Fabry, 2008; Ries et al., 2009). Pteropods living in polar waters will be most affected by a decrease in aragonite saturation state (Comeau et al., 2012), and live shell dissolution has been reported in the Southern Ocean (Bednaršek et al., 2012). However, the response of marine organisms and ecosystems to ocean acidification is still unclear and also depends on other factors, such as nutrient availability (Hoppe et al., 2013), species interactions (Kroeker et al., 2013), and the previous exposure history of an organism to high pCO_2 waters (Lewis et al., 2013). Therefore it is important to characterise the spatial variability of carbonate chemistry in polar oceans in order to determine the environmental conditions that marine organisms currently experience.

The carbonate system in polar oceans has high natural variability (Conrad and Lovenduski, 2015; Kapsenberg et al., 2015) and strong spatial gradients (Bakker et al., 2008; Fransson et al., 2009), which makes it challenging to distinguish natural processes from perturbations resulting from a gradual uptake of anthropogenic CO_2 (Ericson et al., 2014; van Heuven et al., 2011a). In order to predict the future impact of climate change on the polar carbonate system we must therefore understand the interactions between the physical and biogeochemical processes that drive the spatial variability. Biological processes are reported to have a strong influence on variations in DIC, pH and Ω. During summer months polar surface waters have typically higher calcium carbonate saturations states due to intense primary productivity, as shown in the Arctic shelf seas including the Chukchi Sea (Bates et al., 2009), the Amundsen Gulf (Chierici et al., 2011) and the Barents Sea Opening (Tynan et al., 2014), and also in western (Mattsdotter-Björk et al., 2014) and eastern Antarctica (Roden et al., 2013). This results in more favourable pH and Ω conditions for organisms during summer. Robbins et al. (2013) found sea-ice melt to be an important driver for the carbonate system in areas with low biological activity in the Arctic, such as the Canada Basin and Beaufort Sea. Glacial melt (Evans et al., 2014) and river runoff (Mathis et al., 2011) were also found to drive low saturation states in the subpolar Pacific.

In this study, we determine the processes that drive carbonate chemistry, including pH and aragonite saturation state (Ω_{ar}), in the Atlantic sectors of the Arctic and Southern Oceans during their respective summers. A unique aspect of this study is formed by the availability of dissolved iron data, which allows a detailed assessment of the conditions for biological productivity, relevant to CO_2 uptake. Our aim is to focus on the spatial variability of the carbonate system in surface waters. For this, we include the use of water column data to infer changes from the subsurface to surface waters, and determine the processes that result in large horizontal gradients in the study regions. We first present the environmental setting for the cruises (Section 4.1) followed by total alkalinity (TA) and DIC distributions (Section 4.2), before presenting pH and Ω_{ar} distributions (4.3). The physical and biogeochemical processes controlling surface pH and Ω_{ar} are investigated with respect to seasonal changes in the Southern Ocean (5.1) and through horizontal gradients in the Arctic Ocean (5.2). Variable reduction through a principal component analysis (PCA) confirmed the different forcing factors in the two polar oceans (5.3). As the seasonal ice zone is changing rapidly, an improved understanding of how this will affect the carbonate system in these regions is critical. Therefore, we finally focus on these areas and investigate in detail the processes that drive pH and Ω_{ar} in both polar oceans upon sea-ice retreat (5.4). This manuscript, finally, also provides a carbonate chemistry context for other manuscripts in this special issue ("Impacts of surface ocean acidification in polar seas and globally: a field-based approach").

2. Study area

Data were collected on two cruises of the UK Ocean Acidification Research Programme to the polar regions. The cruises covered the Atlantic sectors of the Arctic and Southern Oceans: the Nordic and Barents Seas in the Arctic, and the Scotia and Weddell Seas in the Southern Ocean. The main aim of the cruise programme was to investigate the effects of ocean acidification on biogeochemical processes and polar ecosystems, through field observations across carbonate chemistry gradients and CO_2 perturbation experiments (see Poulton et al. (2016), Rees et al. (2016), Peck et al. (2016), Hartmann et al. (2016), Cavan et al. (2015) and Le Moigne et al. (2015)).

2.1. Arctic

The Nordic Seas connect the Arctic and Atlantic Oceans, and are the site of heat, freshwater and mass exchange between the two basins (Dickson et al., 2008). Warm salty Atlantic waters flow northwards into the Arctic Ocean, and cold fresh Arctic waters southwards, forming a strong natural gradient of water masses (Fig. 1). The Norwegian Atlantic Current (NWAC) splits at the Barents Sea Opening into the West Spitsbergen Current (WSC) which flows northwards into the Arctic Ocean through the Fram Strait, and the North Cape Current (NCC) which feeds Atlantic waters into the Barents Sea (Blindheim and Østerhus, 2005). Part of the WSC recirculates westwards at the Fram Strait and mixes with the southflowing polar waters (Bourke et al., 1988). Polar waters exit the Arctic Ocean on the western side of the Fram Strait and follow the East Greenland Current (EGC) along the Greenland Shelf towards the Denmark Strait (Woodgate et al., 1999). Part of the polar waters from the EGC branch eastwards into the central Nordic Seas as the Jan Mayen Current (Bourke et al., 1992) and the East Iceland Current (Swift and Aagaard, 1981).

Sea-ice cover in the Nordic Seas is largely confined to the EGC, extending as far as the Denmark Strait in winter, and progressively retreating northwards towards the Fram Strait during summer melt. The majority of Arctic sea-ice is exported through the Fram Strait (Kwok et al., 2004) and the high interannual variability of sea-ice cover in the Greenland Sea is correlated to the variability in sea-ice export (Kvingedal, 2005). Unfavourable winds result in low sea-ice cover, while years of low summer Arctic sea-ice cover result in a higher extent and concentration in the Greenland Sea due to easier movement of the Arctic ice mass (Stroeve et al., 2005). In the Barents Sea, sea-ice covers the northern polar waters during winter, and exposes them completely during summer (Vinje, 2001). The winter sea-ice edge has retreated northeastwards over the last decades, due to advection of warm Atlantic waters further north (Shapiro et al., 2003).

The Nordic Seas and Barents Sea are some of the most productive seas in the Arctic Ocean (Sakshaug, 2004) due to a combination of high macronutrient and iron supply, deep winter mixing and extensive ice free regions during summer periods

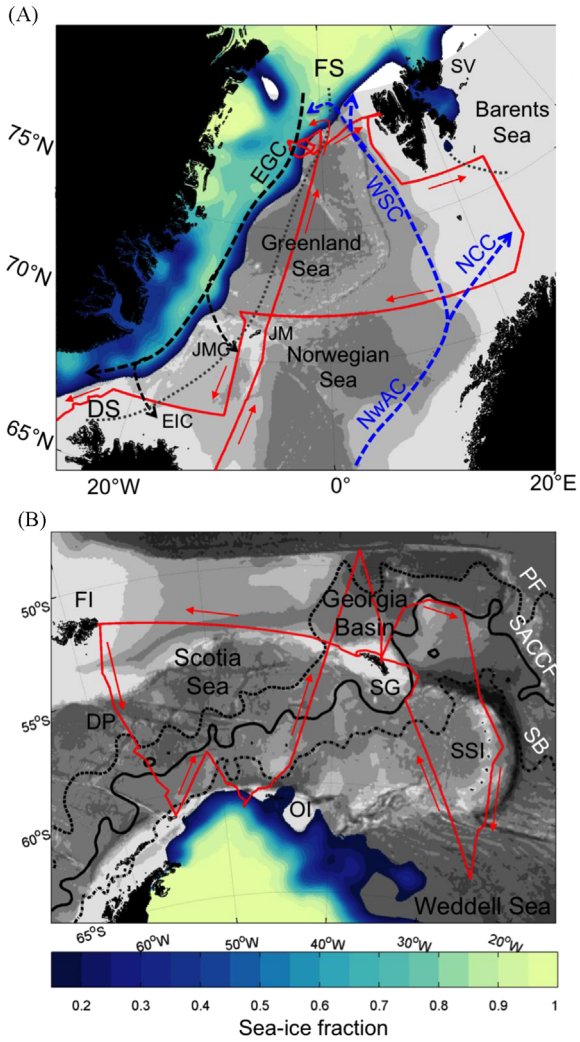

Fig. 1. Maps of the study areas showing cruise tracks (red with arrows indicating direction) plus major currents and fronts. (a) Arctic cruise – blue dashed arrows indicate Atlantic waters and black dashed arrows Polar waters. Dotted grey lines indicate the approximate position of the polar fronts during the cruise [DS: Denmark Strait; FS: Fram Strait, NwAC: Norwegian Atlantic Current; NCC: North Cape Current; WSC: West Spitsbergen Current; JMC: Jan Mayen Current, EIC: East Iceland Current; JM: Jan Mayen; SV: Svalbard]; (b) Southern Ocean cruise showing mean position of the fronts during the cruise (PF: Southern edge of the Polar Front, dotted black line; SACCF: Southern Antarctic Circumpolar Current Front, solid black line; SB: Southern Boundary, dashed black line) [FI: Falkland Islands; SG: South Georgia; SSI: South Sandwich Islands; OI: South Orkney Islands; DP: Drake Passage]. Average sea-ice fraction during the cruises is shaded in blue/cream; bathymetry is shaded in 1000 m intervals, darker shades indicate greater depth. (For interpretation of the references to colour in this figure legend, the reader is referred to the web version of this article.)

creating favourable light conditions. In the seasonal ice zones of the Fram Strait, along the East Greenland Shelf and in the Northern Barents Sea, sea-ice edge blooms are short-lived but intense, with high biomass accumulation due to strong stratification (Carmack and Wassmann, 2006). In contrast in the deep basins of the Nordic Seas and the Southern Barents, where freshwater inputs are minimal, increased vertical mixing results in lower chlorophyll concentrations that can be sustained over a prolonged period (Carmack and Wassmann, 2006).

2.2. Southern Ocean

The eastward-flowing Antarctic Circumpolar Current (ACC) dominates the circulation in the Southern Ocean, facilitating exchange with the major ocean basins (Nowlin and Klinck, 1986). Wind-driven upwelling in this region is a key component of the meridional overturning circulation (Marshall and Speer, 2012). The ACC separates sub-tropical waters to the north from Antarctic waters to the south. It consists of current jets associated with north to south fronts in water mass properties: the Sub-Antarctic Front (SAF), the Polar Front (PF) and the Southern Antarctic Circumpolar Current front (SACCF) (Orsi et al., 1995). The ACC and associated water masses occupy most of the Scotia Sea. The southern boundary (SB) of the ACC, south of the SACCF, marks the southern limit to these water masses. South of the ACC lies the Weddell Sea, separated from the ACC by the Weddell-Scotia Confluence, a mixture of waters from the Scotia and Weddell Seas with shelf water from the Antarctic Peninsula (Whitworth et al., 1994).

During austral winter, sea ice fully covers the Weddell Sea and the south-eastern part of the Scotia Sea, including the South Sandwich Islands. Summer sea-ice melt exposes the eastern Weddell Sea, while the western side remains covered throughout the year (Ackley, 1981). However, recent years have seen anomalously high sea-ice concentrations in the Weddell Sea (NSIDC; http://nsidc.org/data/seaice_index), with summer sea-ice extending further north and west, and this was also the case in 2013 (Reid et al., 2015).

Large parts of the Southern Ocean are classified as 'high-nitrate low-chlorophyll' (HNLC), which is related to limitation of phytoplankton growth by a limited supply of iron in these macronutrient replete waters (de Baar et al., 1995). The Scotia and Weddell Seas have a relative high productivity compared to rest of the HNLC waters in the Southern Ocean (Korb et al., 2005). Favourable topography and eddies supply iron to the region, facilitating bloom formation (Kahru et al., 2007; Park et al., 2010). In particular, the South Georgia bloom in the Scotia Sea is the largest and most prolonged bloom in the Southern Ocean (Korb et al., 2008).

3. Methods

3.1. Sampling

The two polar cruises were conducted on board the RRS *James Clark Ross*. The Arctic cruise, JR271 (1st June–2nd July 2012), covered the Nordic Seas, Barents Sea and Denmark Strait, and the Southern Ocean cruise, JR274 (9th January–12th February 2013), covered the Scotia and Weddell Seas.

We collected water column and underway surface water samples for all variables, but the focus of this paper is on spatial variability of surface waters. Water column data was used to infer changes in surface water and is not fully described (see Supplementary information). In the interest of clarity it is worth mentioning that unless specifically stated, description of variables throughout the paper refers to surface water properties (<6 m). Spatial resolution of surface water sampling during the Arctic cruise was higher than during the Southern Ocean cruise, due to the successful deployment of a pH sensor during that cruise, as detailed below. This sensor was also deployed during the Southern Ocean, but due to technical issues the data was not of sufficiently high quality and therefore not used for the analysis in this study.

Surface ocean temperature and salinity from the underway seawater supply (intake at ca. 6 m depth) were logged continuously using a shipboard thermosalinograph (SBE 45, SeaBird Electronics, Inc.). Measurements were averaged to one minute resolution, and calibrated using the conductivity-temperature-depth (CTD) profiler data. During the Arctic cruise, a spectrophotometric pH instrument sampled every 6 min from the ship's underway seawater supply; samples for surface DIC and TA were

collected every one-to-two hours from this supply. Discrete samples for DIC and TA in the water column were obtained from the CTD casts using 20 L Ocean Test Equipment bottles. All DIC and TA samples were collected into 250 mL Schott Duran borosilicate glass bottles using silicone tubing and poisoned with 50 μL of saturated mercuric chloride solution after creating a 2.5 mL air headspace. Samples were immediately sealed shut with ground glass stoppers and stored in the dark until analysis.

3.2. Carbonate system measurements

3.2.1. DIC and TA

All Arctic samples were analysed on-board within 36 h of collection using a VINDTA 3C instrument. The DIC was measured by coulometric titration and TA by potentiometric titration and calculated using a modified Gran plot approach (Bradshaw et al., 1981). Due to malfunctioning of the coulometer on the VINDTA 3C during the Southern Ocean cruise, one-third of samples were analysed on-board with a DIC analyser which uses non-dispersive infrared detection (Apollo SciTech AS-C3 with a LI-COR 7000), with subsequent TA analysis on the VINDTA 3C system. The remainder of the samples were analysed at the National Oceanography Centre, Southampton (NOCS) using a VINDTA 3C instrument for both DIC and TA. Measurements were calibrated using certified reference material (batch 117 in the Arctic, batches 119 and 120 in the Southern Ocean) obtained from A.G. Dickson (Scripps Institution of Oceanography, USA). The $1\boldsymbol{\sigma}$ measurement precision was calculated as the absolute difference between sample duplicates divided by $2/\sqrt{\pi}$ (Thompson and Howarth, 1973), and was ± 3.8 and ± 1.7 μmol kg^{-1} for DIC and TA, respectively, for the Arctic Ocean. For the Southern Ocean, overall DIC precision was ± 1.3 μmol kg^{-1} for measurements with the Apollo and ± 3 μmol kg^{-1} for measurements with the VINDTA; TA precision was ± 2 μmol kg^{-1}.

3.2.2. pH analysis

The measurement technique was based on a colorimetric method using thymol blue as a pH indicator (Rérolle et al., 2012). pH was determined on the total pH scale. Measurements were made every 6 min with a precision of ± 0.001 pH (Rérolle et al., 2013). Bottles of tris pH buffer and DIC/TA CRM provided by Prof. A.G. Dickson (Scripps Institution of Oceanography, USA) were analyzed at 25 °C during the cruise to determine the accuracy and stability of the pH measurements. No trend was detected in the tris buffer pH measurements ($pH_{meas} - pH_{tris}$: 0.003, 0.006, 0.003, 0.002) and the accuracy was determined to be 0.006 pH units. The thymol blue extinction coefficients were determined in the laboratory and the indicator's dissociation constant taken from Zhang and Byrne (1996) (cf. Rérolle et al., 2013).

3.2.3. Carbonate system calculations

The full suite of carbonate system variables was calculated from the discrete DIC and TA measurements, with accompanying phosphate, silicate, temperature and salinity data, using version 1.1 of the CO_2SYS programme for MATLAB (MathWorks) (Van Heuven et al., 2011b). We used the carbonic acid dissociation constants of Mehrbach et al. (1973) refitted by Dickson and Millero (1987), the boric acid dissociation constant of Dickson (1990a), the bisulphate ion acidity constant of Dickson (1990b) and the boron-to-chlorinity ratio of Lee et al. (2010). pH is reported using the Total pH scale ($pH = -\log_{10}([H^+] + [HSO_4^-])$). The carbonic acid dissociation constants of Mehrbach et al. (MER) are only characterised above temperatures of 2 °C, while temperatures below this were observed in some regions in both the Arctic and Southern Ocean cruises. We tested the validity of the constants of MER for the cold water regions by comparing pH and Ω_{ar} values obtained using dissociation constants characterized for low temperatures (Goyet and Poisson, 1989 (GOY); Lueker et al., 2000 (LUK); Roy et al., 1993 (ROY)). Studies into internal consistency of measurements of carbonate chemistry variables have shown that the constants of ROY yield better results in cold polar waters (Chierici and Fransson, 2009), while the constants of MER provide better results in warmer waters (Lee et al., 2000). In an intercomparison study, Ribas-Ribas et al. (2014) found that for warmer water, calculations using constants by ROY were inconsistent with those by MER and LUK. Our dataset includes results from areas with cold waters ($T < 2$ °C), but the majority of our datapoints (more than 65%) were in areas with sea-surface temperature above 2 °C. While we found no significant difference when using either ROY, MER, LUK or GOY constants, with the maximum difference (0.004 for pH and 0.01 for Ω_{ar}) within calculation error, we decided to use the constants of MER since the mean temperature during both cruises was above 2 °C (Arctic = 4.1 °C and S. Ocean = 2.4 °C).

A salinity-temperature relationship for TA was derived for the Arctic cruise from discrete underway surface water samples ($TA = 127.3S - 1.08\ S^2 - 10.3T + 1.27\ T^2 - 801$, Root Mean Squared Error = 10.2 μmol kg^{-1}), and this was used to increase the spatial resolution of surface water TA using the high-resolution temperature and salinity data of the underway logger. The calculated TA was matched with the underway pH measurements, and used to calculate all other carbonate system variables in the Arctic surface ocean, again using CO_2SYS, with the same constants as for the discrete DIC and TA samples.

3.3. Ancillary data

3.3.1. Oxygen, nutrients and iron

Water samples for dissolved oxygen (DO) were collected from selected CTD casts to calibrate the CTD oxygen sensor. Seawater was drawn directly into volume-calibrated glass bottles via Tygon tubing and then fixed by addition of manganese chloride and sodium hydroxide/sodium iodide solutions. After thorough mixing and time for the fixing reaction to complete (at least 1 h) DO was determined by Winkler titration, using a Winkler Ω-Metrohm titration unit (794 DMS Titrino) with amperometric determination of the titration end-point (Culberson and Huang, 1987), and reagents prepared prior to cruise following Dickson (1994). Precision was ± 1 μM or better. Apparent oxygen utilisation (AOU) for the water column profiles was calculated as the difference between the oxygen concentration expected at equilibrium with the atmosphere at the temperature and salinity observed in-situ, and the oxygen concentration measured.

Discrete samples for inorganic nutrients (nitrate + nitrite, phosphate and silicate) were collected from CTD casts and the underway water supply at the same intervals as the DIC and TA samples. Inorganic nutrients were measured using a Skalar San^{plus} segmented-flow autoanalyser following Kirkwood (1996). Precision was ± 0.04 μM for nitrate + nitrite, ± 0.007 μM for phosphate and ± 0.01 μM for silicate, and accuracy was 0.003 μM, 0.001 μM and 0.002 μM respectively.

Samples for dissolved iron were collected using trace metal clean towed fish positioned at 3–4 m depth, an acid-cleaned PVC hose and a Teflon bellows pump (Almatec A15) (Achterberg et al., 2001). The seawater was pumped into a clean container and filtered using a 0.2 μm poresize filter cartridge (Sarobran P300, Sartorius). The samples were stored in acid cleaned 125 mL low density polyethylene bottles (Nalgene) and acidified on-board. Sample analysis was conducted at NOCS using an isotope dilution technique in conjunction with ICP-MS analysis (Element IIXR, Thermo Fisher Scientific), following Milne et al. (2010). Seawater standards (SAFe D2 and GEOTRACES D) were preconcentrated and

analyzed with each batch of samples, in order to validate our sample concentration. Values obtained for the seawater standards agreed with reported values for the GEOTRACES and the SAFe standard seawater (SAFe D2: 0.92 ± 0.02 nmol Fe L^{-1} (consensus value 0.90 ± 0.02 nmol Fe L^{-1}), GEOTRACES D: 1.00 ± 0.04 nmol Fe L^{-1} (consensus value 0.95 ± 0.05 nmol Fe L^{-1})). The precision for replicate analyses was between 1% and 3%.

3.3.2. Stable isotopes of DIC

During the Arctic cruise (JR271), samples were collected to measure the stable isotopic composition of DIC ($\delta^{13}C_{DIC}$) following the same procedure as for DIC and TA (Section 3.1) except that smaller, 100 mL bottles, were used and these were poisoned with 20 μL of saturated mercuric chloride solution and had 1 mL air headspace. These samples were analysed at the Scottish Universities Environmental Research Centre – Isotope Community Support Facility (SUERC-ICSF) in East Kilbride (UK) using a mass spectrometer (Delta V, Thermo Fisher Scientific) coupled to a sample introduction system (Gasbench 2, Thermo Fisher Scientific). The measurements are reported relative to the Vienna Peedee Belemnite (V-PDB) international standard (Coplen, 1995), and have a $1\boldsymbol{\sigma}$ precision – based on duplicates – of 0.1‰. Further details of the analytical and calibration procedures can be found in Humphreys et al. (2015).

3.3.3. Satellite data on sea ice and dynamic topography

Daily fields of sea ice concentration were produced from satellite data by the Operational Sea Surface Temperature and Sea Ice analysis (OSTIA; Donlon et al., 2012) run by the UK Meteorological Office. The sea ice data at a spatial resolution of 1/20° were spatially interpolated onto the cruise track to provide a time series of daily sea ice concentrations. The mean positions of the ACC fronts for the Southern Ocean study region were defined from satellite-derived sea surface height fields (Venables et al. (2012). Daily fields of near-real time absolute dynamic topography, gridded at 1/4° resolution, were obtained from Aviso for the period of the cruise (Rio and Hernandez, 2004). The mean of the daily fields was contoured to represent the frontal positions.

3.4. Seasonal changes in the Southern Ocean

The subsurface Winter Water (WW) layer south of the Polar Front in the Southern Ocean was used to estimate the sea surface distributions of variables in the preceding winter, and so calculate seasonal changes (Jennings et al., 1984). By using the core of the winter water layer the effects of diffusion and vertical mixing on physicochemical properties was minimised. However, surface waters can be subject to stronger advection than subsurface waters, and the winter water layer then may not be representative of the winter conditions of the surface water directly above it. The temperature of the winter water layer in the southern part of the cruise track was colder than waters further north (Fig. S1) and was close to the freezing point of seawater ($T < -1.5$ °C), reflecting the presence of sea-ice during the previous winter ($>90\%$ concentration; Fig. S2). Therefore it is valid to assume that winter water layer in the Weddell Sea represents conditions during the previous winter. Winter water temperatures in the ACC in the northern part of our transect ranged between –0.8 °C and 1.9 °C (Fig. S3), becoming warmer from south to north, in agreement with climatological temperature distributions for August across the Scotia Sea (-1.5 °C to 2 °C; Schmidtko et al., 2013; http://www.pmel.noaa.gov/mimoc) (Fig. S3). Therefore these temperatures agree over broad spatial scales and we assume in our WW analysis that advection of the surface and subsurface waters was similar and that the subsurface WW waters reflect surface water conditions in the preceding winter.

The depth of the subsurface potential temperature minimum that defines the WW was interpolated – using a piecewise cubic hermite interpolating polynomial (PCHIP) implemented by MATLAB (MathWorks) – from CTD sensor measurements at each station, and the value of each variable at that depth was taken as the WW value (Dong et al., 2008). The net differences in TA, DIC and dissolved inorganic nitrate (DIN) (ΔTA, ΔDIC and ΔDIN) between the WW and the surface layer can therefore be calculated:

$$\Delta TA = TA_{surf} - TA_{WW}$$
$$\Delta DIC = DIC_{surf} - DIC_{WW}$$
$$\Delta DIN = DIN_{surf} - DIN_{WW}$$

where TA_{WW}, DIC_{WW} and DIN_{WW} are the observed values of TA, DIC and DIN in the WW layer, and TA_{surf}, DIC_{surf} and DIN_{surf} are the same for the surface waters sampled in the Southern Ocean. These surface values for each sampling station are the mean of all measurements in the mixed layer at that station for each variable (mixed layer depth defined as the depth where potential density differs from that at the surface by 0.05 kg m^{-3}). The changes from WW values to those observed in the surface during cruise JR274 were attributed to several processes: freshwater balance (fw), primary production and respiration (bio), calcium carbonate production and dissolution (ca) and temperature (temp). The residual was attributed to physical processes such as air-sea exchange, diffusion, advection, and upwelling (resid).

The winter-to-summer changes in TA, DIC and DIN driven by freshwater inputs and losses (ΔTA_{fw}, ΔDIC_{fw} and ΔDIN_{fw}) can be estimated using the observed changes in salinity between the WW layer and the surface. Firstly, the relative volume of freshwater added or lost (V_0) is calculated:

$$V_0 = \frac{S_{WW} - S_{surf}}{S_{surf}}$$

where S_{WW} and S_{surf} are the observed values of S in the WW layer and in the surface water, respectively. This V_0 is then used to determine the change in other variables associated with this freshwater addition, assuming that the freshwater had zero TA, DIC, DIN and S:

$$\Delta TA_{fw} = -\frac{V_0 \cdot TA_{WW}}{1+V_0}$$
$$\Delta DIC_{fw} = -\frac{V_0 \cdot DIC_{WW}}{1+V_0}$$
$$\Delta DIN_{fw} = -\frac{V_0 \cdot DIN_{WW}}{1+V_0}$$

The biological change in DIN (ΔDIN_{bio}) can then be estimated as the difference between ΔDIN_{fw} and the total change in DIN between the WW and surface layers (ΔDIN):

$$\Delta DIN_{bio} = \Delta DIN - \Delta DIN_{fw}$$

This can be used to estimate the biological component (ΔDIC_{bio}) of the total WW to surface water change in DIC (ΔDIC):

$$\Delta DIC_{bio} = \Delta DIN_{bio} \bullet R_{C/N}$$

where $R_{C/N}$ is the adjusted 'Redfield' ratio between carbon and nitrogen in particulate organic matter (POM), which takes a value of 117/16 (Anderson and Sarmiento, 1994). We can similarly estimate the biological component of the TA change (ΔTA_{bio}):

$$\Delta TA_{bio} = -\Delta DIN_{bio} \bullet (1 + R_{\frac{P}{N}} + 2R_{\frac{S}{N}})$$

where $R_{P/N}$ and $R_{S/N}$ are adjusted Redfield ratios between phosphorus, sulphur and nitrogen in particulate organic matter (POM). The term $(1+R_{P/N}+2R_{S/N})$ takes a value of 1.36 (Wolf-Gladrow et al., 2007).

After removal of the freshwater and biological components, the residual change in TA (ΔTA_{resid}) can be attributed to calcium

carbonate production and dissolution (ΔTA_{ca}), and the contribution of advection. We assume that the latter is negligible, so ΔTA_{resid} can be assumed to be approximately equal to ΔTA_{ca}:

$$\Delta TA_{resid} = \Delta TA - \Delta TA_{fw} - \Delta TA_{bio} \approx \Delta TA_{ca}$$

The effect of calcification on DIC (ΔDIC_{ca}) is equal to half of ΔTA_{ca} (Wolf-Gladrow et al., 2007):

$$\Delta DIC_{ca} = \frac{\Delta TA_{ca}}{2}$$

Finally, the residual change in DIC (ΔDIC_{resid}) can be attributed to physical processes and is calculated as follows:

$$\Delta DIC_{resid} = \Delta DIC - \Delta DIC_{fw} - \Delta DIC_{bio} - \Delta DIC_{ca}$$

The effect of each process on aragonite and calcite saturation states (collectively referred to as Ω) and pH was then quantified. First, Ω and pH were calculated using TA_{WW}, DIC_{WW}, S_{WW}, and WW temperature (T_{WW}) and nutrient concentrations, to represent the surface water at the previous winter. These results were compared with the same calculation carried out using the TA_{WW} and DIC_{WW} adjusted for each process. For example, to determine the freshwater impact on Ω and pH, these variables were calculated from ($TA_{WW} - \Delta TA_{fw}$) and ($DIC_{WW} - \Delta DIC_{fw}$), using the observed S_{surf} and surface temperature (T_{surf}) and nutrient concentrations, and compared with values calculated directly from WW observations.

3.5. Statistical analysis

Principal component analysis (PCA) of standardized variables was performed using MATLAB. This approach provides a good representation of variation within the data. In case there are associations between the variables, the first two or three components will usually explain the majority of the variation in the original variables, which can then summarise the patterns in the original data based on a smaller number of components (i.e., variable reduction). Principal component analysis is an ordination in which samples, regarded as points in a high-dimensional variable space (in this study we have 10 variables and thus 10-dimensions with 10 principal component outcomes) are projected onto a best fitting plane. The axes capture as much variability in the original space as possible, and the extent to which the first few PCs allow an accurate representation of the true relationship between samples in the ordinal high-dimensional space is summarised by the percentage variation explained (Clarke and Gorley, 2006).

4. Results

4.1. Environmental setting

The water masses encountered in the surface ocean during the cruises and their physicochemical properties are presented in Table 1. Warm salty Atlantic Waters (AW; $T > 2$ °C, $S > 34.9$), were observed in the Norwegian Seas, southern Barents Sea and along the west coast of Svalbard (Fig. 1a). Recirculating Atlantic Waters (rAW; $T < 2$ °C, $S > 34.8$) were found in the Greenland Sea. Two major fronts, evident from salinity variations (Cottier et al., 2014), separated the Atlantic waters from cold Polar waters (defined as all waters with $S < 34.5$): the Polar front in the northernmost region of the Barents Sea (Kostianoy and Nihoul, 2009) and the East Greenland Front in the Fram Strait, northeast of Jan Mayen Island and in the Denmark Strait (Rudels et al., 2005). Very cold Polar Surface Water (PSW; $T < 0$ °C, $S < 34.4$) was found on the western side of the Fram Strait below the ice. Sea-ice melt over the Greenland Shelf and in the Northern Barents Sea, reduced salinity

Table 1
Physicochemical properties of surface waters observed during the Arctic and Southern Ocean Cruises. The average and standard deviation of the variables for each of the water masses/regions is shown in brackets.

	Salinity	Temp. (°C)	NO_3 (μmol kg^{-1})	PO_4 (μmol kg^{-1})	SiO_3 (μmol kg^{-1})	O_2 (μmol kg^{-1})	MLD[a] (m)	pH	TA (μmol kg^{-1})	DIC (μmol kg^{-1})	$\delta^{13}C_{DIC}$ (‰)	pCO_2 (μatm)	Ω_{ca}	Ω_{ar}
Arctic														
AW[b]	35.0 (0.1)	6.0 (1.8)	3.7 (2.6)	0.3 (0.2)	2.2 (1.5)	338 (26)	27 (12)	8.21 (0.06)	2316 (17)	2093 (29)	1.6 (0.4)	276 (40)	3.7 (0.4)	2.3 (0. 2)
rAW[b]	34.9 (0.1)	3.7 (4.2)	4.4 (3.6)	0.3 (0.2)	1.3 (1.6)	344 (21)	22 (9)	8.18 (0.05)	2305 (7)	2108 (33)	1.2 (0.1)	293 (35)	3.2 (0.5)	2.0 (0.3)
PSW[b]	32.6 (0.4)	−1.3 (0.2)	5.3 (0.6)	0.9 (0.1)	12.4 (1.9)	367 (8)	10 (5)	8.10 (0.08)	2212 (22)	2112 (25)	0.9 (0.3)	280 (55)	2.5 (0.5)	1.6 (0.3)
wPSW[b]	33.9 (0.9)	2.7 (1.8)	1.2 (2.1)	0.2 (0.1)	1.2 (1.6)	365 (15)	17 (12)	8.28 (0.08)	2251 (50)	2013 (53)	2.5 (0.1)	209 (46)	3.8 (0.5)	2.4 (0.3)
NwCC[c]	34.6 (0.1)	7.4 (0.2)	1.4 (1.5)	0.2 (0.1)	0.6 (0.8)	325 (1)	25 (2)	8.20 (0.03)	2310 (6)	2079 (16)	1.7 (0)	281 (18)	3.8 (0.2)	2.4 (0.1)
KF[d]	34.5 (0.1)	4.7 (0.6)	0.3 (0)	0.1 (0)	0.0 (0)	-	13 (7)	8.27 (0.02)	2279 (7)	2052 (8)	1.6 (0)	245 (9)	3.7 (0.1)	2.4 (0.1)
S.Ocean[e]														
PFZ	33.9 (0.1)	5.4 (1.3)	18.4 (3.0)	1.4 (0.3)	5.4 (2.4)	321 (13)	58 (9)	8.07 (0.09)	2274 (21)	2113 (22)	-	378 (88)	2.8 (0.5)	1.8 (0.3)
SZ	33.9 (0.1)	3.2 (0.8)	17.8 (4.6)	1.1 (0.4)	13.0 (5.3)	349 (14)	57 (14)	8.10 (0.10)	2288 (17)	2130 (34)	-	349 (87)	2.8 (0.6)	1.8 (0.4)
AZ	33.8 (0.2)	1.8 (0.9)	21.0 (1.8)	1.4 (0.2)	30.2 (12.3)	345 (11)	37 (12)	8.12 (0.06)	2296 (17)	2141 (23)	-	321 (53)	2.8 (0.4)	1.7 (0.2)
WS	33.6 (0.2)	0.2 (0.7)	20.8 (3.7)	1.4 (0.3)	64.7 (9.4)	356 (11)	29 (8)	8.17 (0.06)	2298 (17)	2132 (29)	-	281 (42)	2.9 (0.4)	1.8 (0.2)

AW: Atlantic Water; rAW: recirculating Atlantic Water; PSW: Polar Surface Waters; wPSW: warm Polar Surface Water; NwCC: Norwegian Coastal Current; KF: Kongsfjorden surface water; SAZ: Subantarctic Zone; PFZ: Polar Frontal Zone; SZ: Southern Zone; AZ: Antarctic Zone; WS: Weddell Sea.
Water mass classification according to:

[a] Mixed layer depth; calculated as shallowest depth corresponding to a density difference ($\Delta\sigma_t$) with the surface waters of more than 0.125 (Monterey and Levitus, 1997) for the Arctic and 0.05 for the Southern Ocean (Venables et al., 2013).

[b] Rudels et al. (2005) and Rudels et al. (2002).

[c] Loeng (1991).

[d] Svendsen et al. (2002).

[e] Venables et al. (2012).

and contributed to the formation of warm Polar Surface Water (wPSW; $T > 0$ °C, $S < 34.5$) in these areas. Glacial melt lowered salinity in Kongsfjorden in Svalbard ($S < 34.7$) (Svendsen et al., 2002), and the reduced salinity signal ($S < 34.7$) in the southernmost region of the Barents Sea transect is characteristic of the freshwater influenced Norwegian Coastal Current (Loeng, 1991).

In the Southern Ocean, the ACC defined a clear north–south trend in surface water mass properties (Table 1). The region is divided into water mass zones according to the temperature-salinity relationships, separated by fronts approximated from surface dynamic height (Fig. 1b) (Venables et al., 2012). The Polar Frontal Zone (PFZ), between the sub-Antarctic Front and the Polar front, the Southern Zone (SZ), between the Polar front and southern Antarctic Circumpolar Current front, and the Antarctic Zone (AZ) between the SACCF and the Southern Boundary, form the ACC. South of this lies the Weddell Scotia Confluence and Weddell Sea (WS). Salinity only varied slightly across the ACC ($S \sim 33.9$), but temperature gradually decreased southwards (Table 1) from the still relatively warm waters of the PFZ (4.5 °C), through the SZ (3.2 °C) to the colder AZ (1.8 °C). The coldest waters were found in the WS (0.2 °C), where sea-ice melt had lowered salinity ($S = 33.6$).

The low nutrient concentrations in the Arctic contrasted with the high levels in the Southern Ocean (Table 1). In the Arctic, nitrate concentrations were generally low (< 5 μmol kg^{-1}) with near depletion (< 2 μmol kg^{-1}) in the warm PSW, NCC and Kongsfjorden. High silicate concentrations (up to 12 μmol kg^{-1}) and low nitrate-to-phosphate ratios indicate the Pacific origin of the PSW of the EGC found in the Fram Strait (Jones et al., 2008b). In the Southern Ocean, nitrate concentrations were high (> 18 μmol kg^{-1}), although lower concentrations (> 10 μmol kg^{-1}) were observed around South Georgia and the South Sandwich Islands. Silicate concentrations increased from ca. 5 μmol kg^{-1} in the PFZ to ca. 65 μmol kg^{-1} in the Weddell Sea, reflecting the pronounced and also preferential uptake of silicate by diatoms in Southern Ocean waters (Hutchins and Bruland, 1998; Takeda, 1998).

4.2. Surface ocean TA and DIC

4.2.1. Total alkalinity

Surface water TA and DIC distributions for the Arctic and Southern Ocean cruises are shown in Fig. 2. In the Arctic, higher TA values (ca. 2320 μmol kg^{-1}) corresponded to the AW in the central Norwegian Sea, southern Barents Sea and the region west of Svalbard. Slightly lower TA (2300 μmol kg^{-1} to 2310 μmol kg^{-1}) was found in the AW in the southern Norwegian Sea and Greenland Sea. In the Fram Strait and Denmark Strait the inflow of low salinity polar waters, combined with localised sea ice melt inputs, reduced

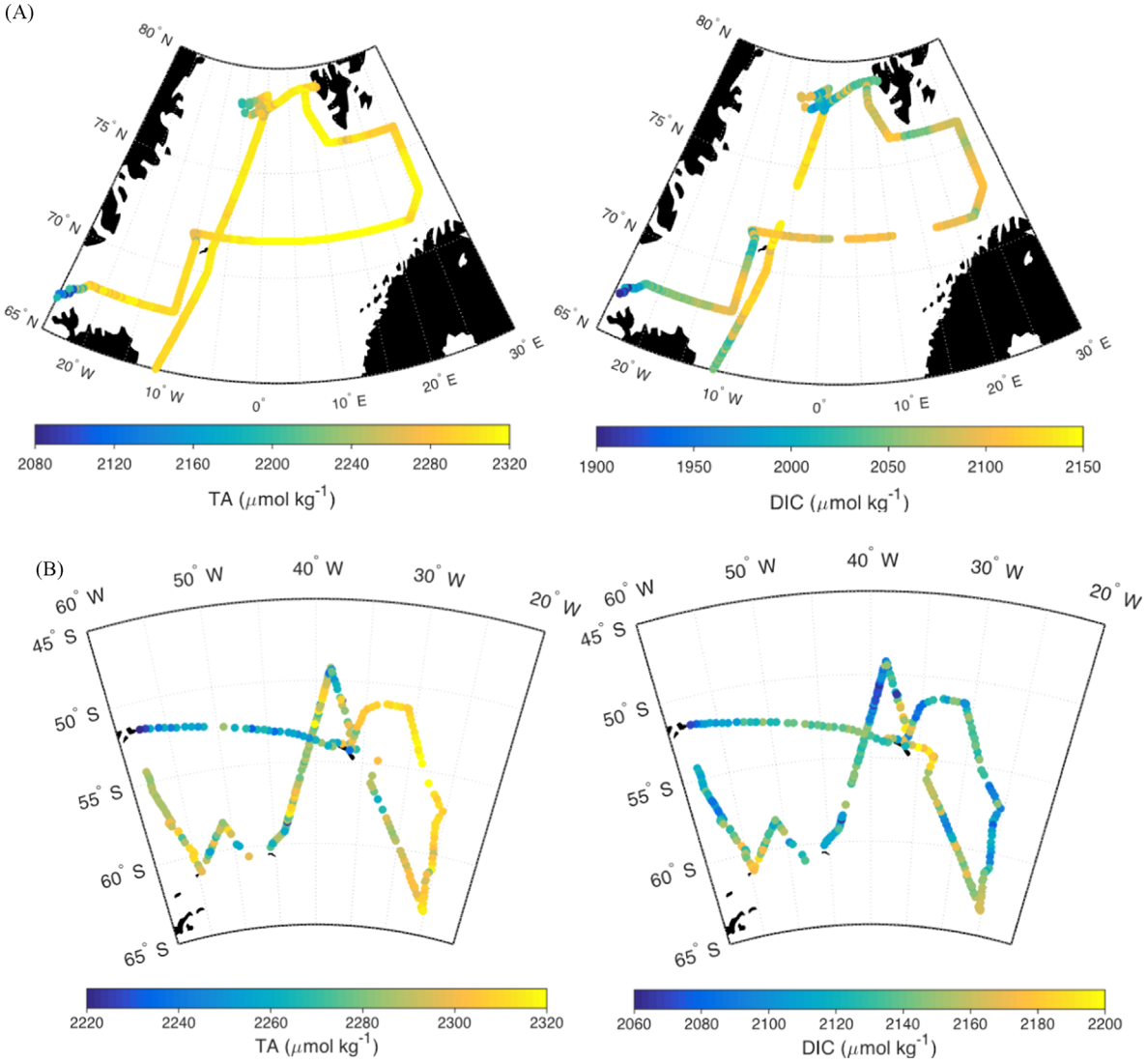

Fig. 2. Surface total alkalinity (TA) and dissolved inorganic carbon (DIC) in (a) the Arctic and (b) the Southern Ocean.

TA to ca. $<2200\ \mu mol\ kg^{-1}$ (Fig. 2a). Freshwater river runoff was observed close to Svalbard, with the enhanced salinity Atlantic water TA signal (ca. $2320\ \mu mol\ kg^{-1}$) decreasing near Kongsfjorden by $\sim 40\ \mu mol\ kg^{-1}$ (79 °N, 10 °E, Fig. 2a). Fresh polar waters also decreased TA (ca. $2280\ \mu mol\ kg^{-1}$) in both the Barents Sea opening (76 °N, 23 °E, Fig. 2a) and off the coast of Jan Mayen (73 °N, 11 °W, Fig. 2a). These values agree with previous reports of higher TA for the Atlantic inflow to the Nordic and Barents Seas, and lower values for colder Arctic waters (Anderson and Dyrssen, 1981).

In the Southern Ocean, the highest TA values were found in the Weddell Sea ($2300–2320\ \mu mol\ kg^{-1}$) and the lowest ($2220–2260\ \mu mol\ kg^{-1}$) in waters north of the Polar Front, in the region between South Georgia and the Falkland Islands (Fig. 2b). This range is similar to that previously reported ($2240–2300\ \mu mol\ kg^{-1}$) for the Weddell-Scotia Confluence area (Jones et al., 2010). While the overall trend was a southwards increase in TA across the circumpolar jets (Table 1), large variability (up to $60\ \mu mol\ kg^{-1}$) was observed within each of the water mass zones (Fig. 3 inset). Sea-ice melt decreased TA around the South Orkney Islands ($2260\ \mu mol\ kg^{-1}$, 60 °S, 45 °W) and in the Weddell Sea area ($2280\ \mu mol\ kg^{-1}$) (Fig. 2b). Terrestrial freshwater inputs close to South Georgia and the Falklands Islands also decreased TA locally ($2220\ \mu mol\ kg^{-1}$) (Fig. 2b). North of South Georgia (50 °S, 40 °W, Fig. 2b) an area of low TA ($2240–2260\ \mu mol\ kg^{-1}$) was also observed (discussed in detail Section 5.1.2).

TA-Salinity relationships indicate conservative mixing in the Arctic, with two different regimes (Fig. 3), as typically observed in the Nordic Seas (Bellerby et al., 2005). Waters on the western side of the Fram Strait had a high zero-salinity end-member (TA_0) of $1230\ \mu mol\ kg^{-1}$, while the remaining areas had a lower TA_0 of $403\ \mu mol\ kg^{-1}$ (Fig. 3). In the Southern Ocean TA-Salinity relationships indicate conservative mixing in the Weddell Sea and southern part of the Scotia Sea with a low alkalinity end-member ($TA_0=236\ \mu mol\ kg^{-1}$) (Fig. 3). In other areas, mixing appears to be non-conservative, with TA concentrations varying by ca. $100\ \mu mol\ kg^{-1}$ for minor variations in salinity (33.8–34.0) (Fig. 3). The different mixing regimes for TA in the surface waters of the Arctic and Southern Oceans indicate control by different processes (Fig. 3). The low TA end-member ($TA_0=430\ \mu mol\ kg^{-1}$) in the Arctic is consistent with sea ice melt ($50–600\ \mu mol\ kg^{-1}$; Rysgaard et al., 2009), while the higher TA end-member ($TA_0=1230\ \mu mol\ kg^{-1}$) is consistent with freshwater inputs from Siberian rivers with elevated TA (ca. $1400\ \mu mol\ kg^{-1}$; Anderson and Dyrssen, 1981). Siberian river runoff is carried by the Transpolar Drift across the Central Arctic and out through the Fram Strait. Polar waters under the ice on the western side of the Fram Strait had high silicate content (ca. $12\ \mu mol\ kg^{-1}$; Table 1), low N:P ratios (ca. 6:1; Table 1), and high TA_0 ($1230\ \mu mol\ kg^{-1}$; Fig. 3), consistent with the transport and mixing of Pacific Ocean-origin waters with Siberian river waters across the Arctic (Jones et al., 2008a). In the Southern Ocean, conservative mixing of TA and salinity in the Weddell Sea and southern Scotia Sea indicates mixing with sea-ice melt ($TA_0=236\ \mu mol\ kg^{-1}$). The non-conservative behaviour of TA in the ACC can be partly explained by the southwards shoaling of deep water masses (Marshall and Speer, 2012). These deep waters have higher TA concentrations, resulting in a gradual increase in TA with dynamic height across the water mass zones in the ACC, with little change in salinity (Fig. 3 inset). However, large variations in TA (ca. 40–$80\ \mu mol\ kg^{-1}$) were observed within the Southern and PF Zones (Fig. 3, inset). The decoupling of TA and salinity in the Southern Ocean observed in the PCA (Fig. S4) is consistent with a non-conservative behaviour and indicates other processes drive these variations in TA. These are discussed in detail in Section 5.1.2.

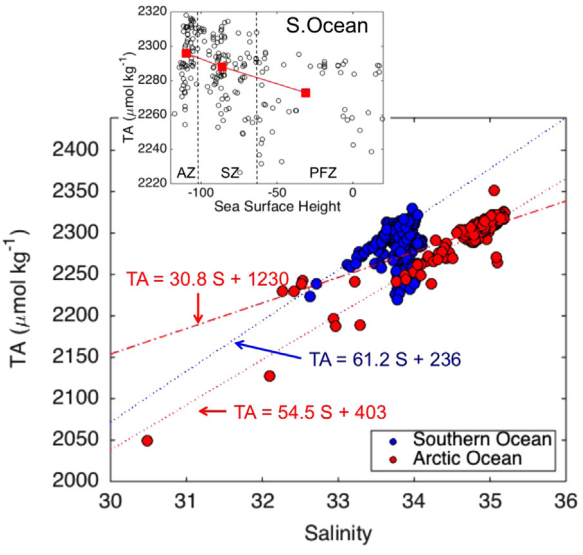

Fig. 3. Relationship between total alkalinity (TA) and salinity for the Arctic and Southern Oceans. Dashed red line indicates the relationship on the western side of the Fram Strait ($r^2=0.96$); dotted red line the relationship for the remaining data ($r^2=0.78$); dotted blue line indicates the relationship for the Weddell Sea in the Southern Ocean ($r^2=0.92$), with other areas showing non-conservative behaviour (Inset: TA concentrations of these areas against sea-surface height; average TA value for each zone is shown in red).

4.2.2. Dissolved inorganic carbon

In the Arctic, the highest surface DIC concentrations ($2120–2140\ \mu mol\ kg^{-1}$) were observed in the Greenland Sea (Fig. 2a), somewhat higher than values reported by Miller et al. (1999) ($2115\ \mu mol\ kg^{-1}$). Atlantic waters in the Norwegian Sea and southern Barents Sea had slightly lower DIC concentrations than those in the Greenland Sea (Fig. 2a) but with larger variability ($2070–2110\ \mu mol\ kg^{-1}$), comparable to values of $2080\ \mu mo\ kg^{-1}$ reported by Findlay et al. (2008). Similarly, large variations were observed on the Atlantic influenced WSC around Svalbard ($2040–2110\ \mu mol\ kg^{-1}$; Fig. 2a). The fresher Norwegian Coastal Current showed lower DIC (ca. $2040\ \mu mol\ kg^{-1}$) off the coast of Norway (72 °N, 24 °E; Fig. 2a). The above values agree with the summer range ($2040–2120\ \mu mol\ kg^{-1}$) reported for Atlantic waters in the Nordic Seas (Falck and Anderson, 2005). Lower DIC concentrations in the northern Barents Sea (ca. $2080\ \mu mol\ kg^{-1}$) were due to the intrusion of Polar waters, which have lower DIC than Atlantic waters (Fig. 2a). Other areas with Polar waters, such as west of Jan Mayen and north of Iceland, also had lower DIC concentrations (ca. $2050\ \mu mol\ kg^{-1}$; Fig. 2a). Particularly large freshwater inputs (salinity close to 30) in the Denmark Strait resulted in very low DIC concentrations ($1900–2000\ \mu mol\ kg^{-1}$; Fig. 2a). Polar waters in the Fram Strait had very large variability (Fig. 2a): those on the westernmost side (5 °W) had high DIC (ca. $2100\ \mu mol\ kg^{-1}$) while those close to the polar front (0 °E) had much lower values (ca. $1950\ \mu mol\ kg^{-1}$). This range is in agreement with values reported for the northern EGC ($1900–2080\ \mu mol\ kg^{-1}$) by Yager et al. (1995).

DIC concentrations ranged between $2100\ \mu mol\ kg^{-1}$ and $2150\ \mu mol\ kg^{-1}$ over much of the Southern Ocean transect (Fig. 2b). Higher DIC concentrations were observed in the southern region of the Drake Passage (ca. $2180\ \mu mol\ kg^{-1}$), southeast of South Georgia (55 °S, 35 °W; $2160–2200\ \mu mol\ kg^{-1}$) and in the southernmost area in the Weddell Sea (ca. $2180\ \mu mol\ kg^{-1}$) (Fig. 2b). Lower DIC concentrations were observed close to the South Sandwich Islands (ca. $2080\ \mu mol\ kg^{-1}$), northwest of South Georgia ($2050–2100\ \mu mol\ kg^{-1}$) and close to the Falkland Islands (ca. $2060\ \mu mol\ kg^{-1}$) (Fig. 2b). The range of values observed is slightly lower than reported previously ($2130–2240\ \mu mol\ kg^{-1}$) for a region spanning the ACC and Weddell Sea (Bakker et al.,

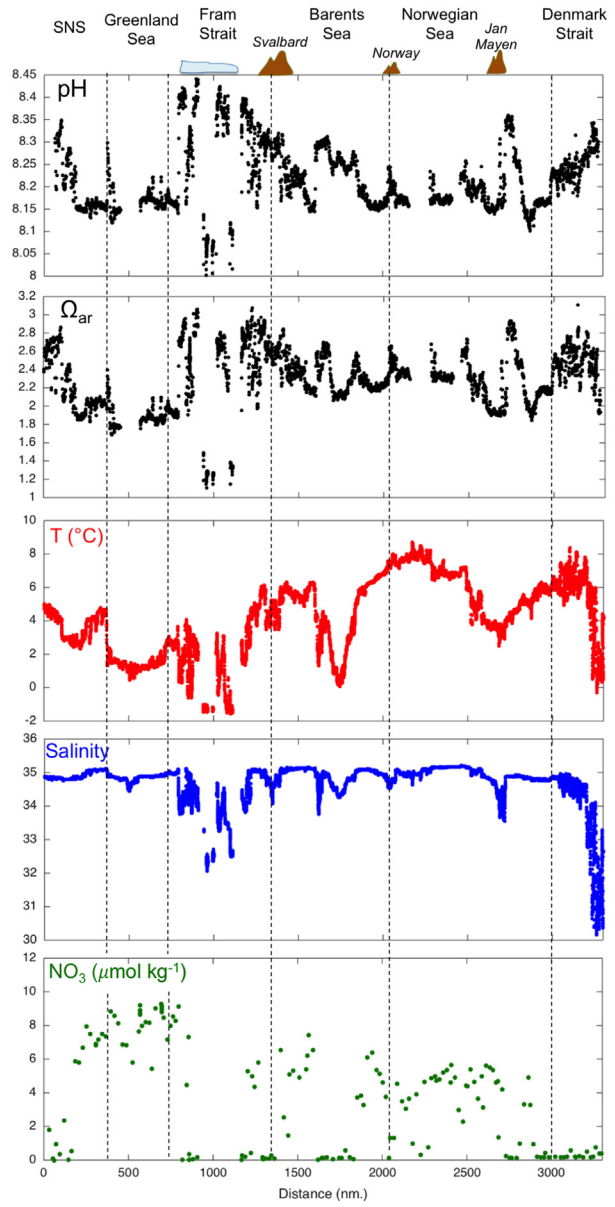

Fig. 4. Variations of pH, Ω_{ar}, temperature, salinity and nitrate concentrations in surface waters (6 m) along the cruise track in the Arctic region. Areas with sea-ice and important landmasses are shown for reference (SNS: Southern Norwegian Sea).

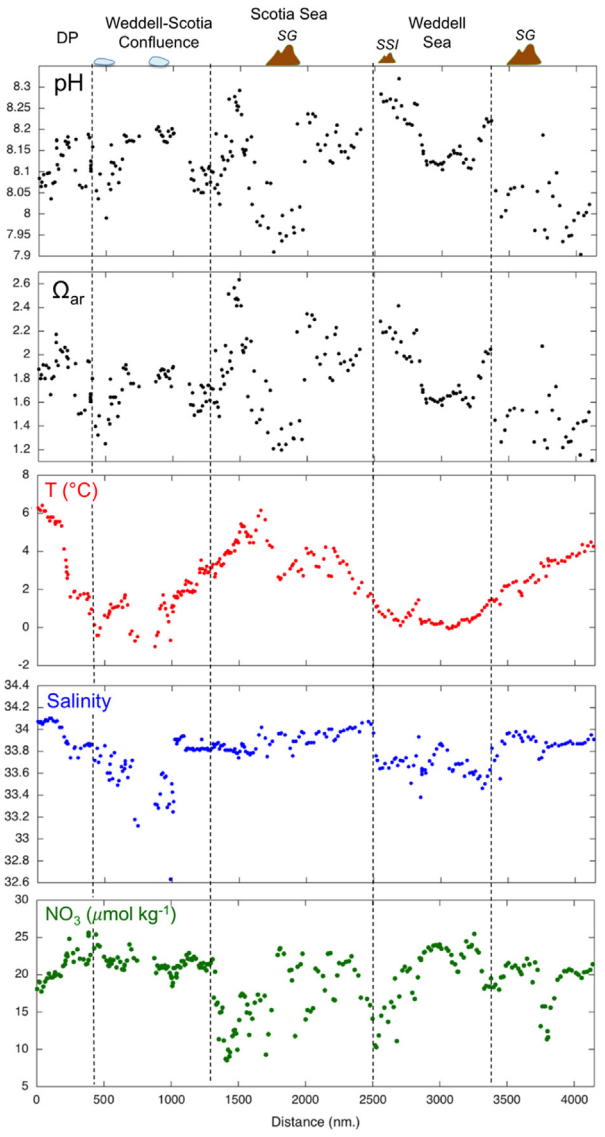

Fig. 5. Variations of pH, Ω_{ar}, temperature, salinity and nutrient concentrations in surface waters (6 m) along the cruise track in the Southern Ocean (SG: South Georgia; SSI: South Sandwich Islands; DP: Drake's passage). Areas with sea-ice and important landmasses are shown for reference.

2008), but within the variability driven by physical and biogeochemical processes of the system.

4.3. Surface pH and Ω_{ar}

In this section we describe the overall distributions and patterns of surface pH and Ω_{ar}, and in Sections 5.1 and 5.2 we discuss the finer-scale variations and processes that drive them. Surface pH and Ω_{ar} were typically lower in the Southern Ocean (Fig. 5) than in the Arctic (Fig. 4). Arctic pH ranged between 8.00 and 8.45, and Ω_{ar} between 1.1 and 3.1. These values are in agreement with previous observations in the Norwegian Sea (Ω_{ar} 2.2–2.6; Skjelvan et al., 2008; Skogen et al., 2014) and at the entrance to the Barents Sea (Ω_{ar} 1.8–2.3 and pH 8.14–8.17; Tynan et al., 2014). In the Southern Ocean pH ranged between 7.90 and 8.30 and Ω_{ar} between 1.2 and 2.6, consistent with summer values found in Western Antarctica (Ω_{ar} 1.1–3.5 and pH 7.9–8.5; Mattsdotter Björk et al., 2014) and in Prydz Bay (Ω_{ar} 1.9 and pH 8.2; Roden et al., 2013). The Arctic spanned a wider range with pronounced differences between the water masses (Fig. 4). The Norwegian Sea, Greenland Sea and southern Barents Sea had pH of ca. 8.15, with higher values in the northern Barents Sea and around Svalbard (8.25–8.30) (Fig. 4). Elevated pH (8.20–8.35) was also observed in the southern part of the Norwegian Sea (Fig. 4), in the Denmark Strait and around Jan Mayen (Fig. 4). The lowest (ca. 8.00) and highest (ca. 8.45) pH values were found in the polar waters of the Fram Strait (Fig. 4). Overall, Ω_{ar} distributions followed a similar pattern to pH distributions (Fig. 4). In the central Norwegian Sea and Barents Sea Ω_{ar} was between 2 and 2.3 on average, while the waters south and west of Svalbard generally had higher Ω_{ar} (2.3–2.8). The Greenland Sea had slightly lower Ω_{ar} (ca. 1.8), although higher values (ca. 2.8) were observed west of Jan Mayen (Fig. 4). The southern Norwegian Sea and the area north of Iceland just east of the Denmark Strait also had higher values (2.2–2.8), but Ω_{ar} decreased to 2.0 in the Denmark Strait. Near corrosive (Ω_{ar} 1.1) waters occupied the westernmost part of the Fram Strait, while the adjacent waters in the middle of the Strait had higher Ω_{ar} values (ca. 3.0) (Fig. 4).

In the Southern Ocean, the overall distribution pattern of pH was similar to Ω_{ar}, although the increase in pH with decreasing temperature across the fronts was not evident in Ω_{ar} values (Table 1). Spatial variability within the water mass zones was observed (Fig. 5). In general, waters north of the polar Front had the lowest pH (8.05–7.90) and Ω_{ar} values (1.7–1.2), but similar low values were also observed north of South Georgia (pH between 8.05 and 7.90 and Ω_{ar} between 1.6 and 1.2) and in the southern part of Drake Passage (pH ca. 8.00 and Ω_{ar} ca. 1.4) (Fig. 5). The highest pH and Ω_{ar} values were observed in the vicinity of the major landmasses, South Georgia (pH up to 8.30 and Ω_{ar} values of 2.6) and the South Sandwich Islands (pH up to 8.30 and Ω_{ar} values of 2.4) (Fig. 5).

5. Discussion

5.1. Seasonal changes in Southern Ocean carbonate chemistry

It is necessary to understand the processes controlling changes in DIC and TA before considering the changes in derived variables like pH, Ω and pCO_2^{sw} that may be of more general interest to the ocean acidification community. In the Southern Ocean, these underlying processes have been inferred from seasonal changes, using the WW layer as a proxy for surface conditions during the preceding winter, as described in Section 3.4 and following e.g. Jennings et al. (1984). The net changes in DIC, TA and DIN from winter (i.e. the WW layer) to summer (i.e. the surface mixed layer during the Southern Ocean cruise) are shown in Fig. 6, with the upper water column DIC and TA distributions shown in Fig. S5. At virtually every sampling station, all of these variables had decreased to some extent from winter to summer (Fig. 6).

Freshwater is known to dilute DIC, TA and DIN, as was observed in the southernmost part of the cruise (Fig. 6a–c), where sea-ice had recently retreated (Fig. S6), and at the single sampling station closest to South Georgia. The size of the freshwater component in these areas relative to the net winter-to-summer change was most important for TA (up to 100%; Fig. 6a), followed by DIC (up to 80%; Fig. 6b) and DIN (up to 18%; Fig. 6c).

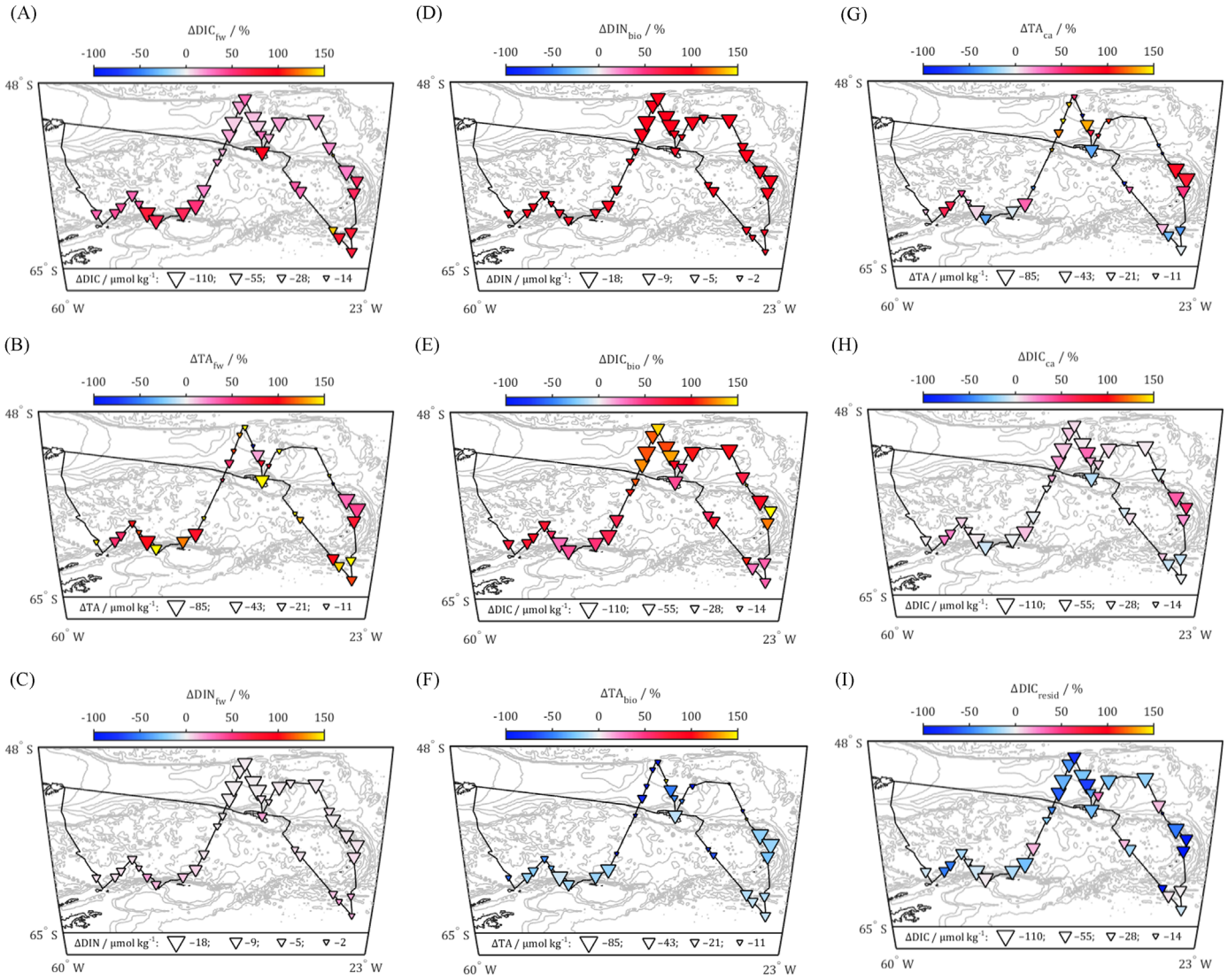

Fig. 6. Components of the net seasonal changes in DIC, TA and DIN, in the Southern Ocean as determined by analysis of the WW layer (Sections 3.4 and 5.1). In each panel, the size of the triangle symbols indicates the net change in the plotted variable from winter to summer at each sampling station. The colour of the symbols indicates the percentage of the net change in the variable that is accounted for by the component indicated in the panel title. Therefore red colours indicate components matching the net change; white indicates a negligible contribution from the component; blue indicates a component acting in the opposite direction to the net change; yellow indicates a component exceeding the net change. Components are fw = freshwater, bio = biological, ca = calcification, and resid = residual (i.e. physical processes), as discussed in the text.

5.1.1. ΔDIN and ΔDIC

The biological component of ΔDIN was high, falling entirely between 80% and 100% of the net winter-to-summer DIN change (Fig. 6d). However, converting this ΔDIN_{bio} into ΔDIC_{bio} revealed additional variation (Fig. 6e). The ΔDIC_{bio} can be considered to take a background value of around 100% of net ΔDIC, and it deviates from this in areas that can be put into two categories. Firstly, the areas that have been identified as having a high freshwater influence – near the recently-retreated ice edge and directly adjacent to South Georgia – had a lower ΔDIC_{bio} relative to net ΔDIC than this background value, with ΔDIC_{bio} reaching a minimum of around 20%. This suggests that in these areas, there had not been any significant primary production in the surface ocean following sea-ice retreat; this is supported by satellite observations of chlorophyll-*a* (chl-*a*), which remained very low in these areas throughout the cruise period (Fig. S7). Conversely, to the north of South Georgia and near the South Sandwich Islands, the ΔDIC_{bio} component was over 150% of the net ΔDIC, indicating enhanced primary productivity and biological uptake of inorganic carbon in these blooms. The HNLC waters of the Southern Ocean are characterised by very low dissolved iron concentrations (typically < 0.2 nM) (see Fig. S8) as a result of low atmospheric Fe supply and an unfavourable N:Fe ratio in deep waters supplied to the surface ocean through deep winter mixing and advective processes with rapid dFe depletion following the on-set of spring phytoplankton blooms (de Baar et al., 1995; Tagliabue et al., 2014). Where inputs of iron do occur, such as in the shelf region surrounding South Georgia and the South Sandwich Islands, they provide a relief to iron limitation of phytoplankton (Nielsdóttir et al., 2012). This was the case during our study, as indicated by enhanced iron in waters downstream (north) of South Georgia (dFe > 0.7 nM) and the South Sandwich Islands (dFe 0.3–0.5 nM), coinciding with enhanced chl-*a* (> 4 mg m^{-3}) in both regions (Figs. S7 and S8). A seasonal depletion of DIC (94 μmol kg^{-1}) and fCO_2 (92 μatm) in the bloom region north of South Georgia has also been reported by Jones et al. (2012).

Further supporting the attribution of this component, in situ measurements of mixed layer particulate organic carbon (POC) production rates during the Southern Ocean cruise revealed relatively high (greater than 7 mmol-C m^{-3} day^{-1}) values at stations in both of the bloom regions (Cavan et al., 2015). However, these instantaneous measurements of POC production are not expected to perfectly mirror the seasonally-integrated changes that are measured by ΔDIC_{bio}, because of the different timescales.

5.1.2. ΔTA

The ΔTA_{bio} was mostly negative with respect to net ΔTA – that is, the biological impact on TA – excluding calcification – had been to increase TA (Fig. 6f). The most extreme ΔTA_{bio} values, relative to net ΔTA, were associated with the bloom to the north of South Georgia. The ΔTA_{bio} was a smaller fraction of net ΔTA in the South Sandwich Islands bloom because of the higher net ΔTA there. Subtracting the components ΔTA_{fw} and ΔTA_{bio} from net ΔTA leaves a residual that can be attributed to calcium carbonate precipitation and dissolution, ΔTA_{ca}.

As a fraction of net ΔTA, the ΔTA_{ca} has a more complex pattern than the other components so far discussed (Fig. 6g). The highest values, sometimes exceeding 100%, were observed in the blooms to the north of South Georgia and near the South Sandwich Islands, and values near 100% were observed in the southwestern part of the cruise. Satellite observations provide some evidence of the presence of particulate inorganic carbon (PIC) production in this area during and immediately preceding the cruise (Fig. S7b). A third independent line of evidence is that relatively high *in situ* calcification rates (greater than 40 μmol C m^{-3} day^{-1}) were measured during the cruise at stations in the South Georgia and South Sandwich Islands bloom (A. Poulton, pers. comm.). The different lines of evidence do not agree in all places; low in-situ calcification rates were observed in the southwestern part of the cruise (although, as described for the POC production rate measurements, this does not prove that calcification had not occurred there since the preceding winter).

Satellite observations of high PIC concentrations (Hopkins et al., 2015) which are indicative of preceding enhanced rates of calcification, and in-situ sampling (Hinz et al., 2012), have shown that elevated abundances of the coccolithophore *Emiliania huxleyi* (200 cells mL^{-1}) in the vicinity of South Georgia can be sustained over a prolonged period. Northwest of South Georgia, the area of low current speed within the cyclonic flow around the Georgia Basin acts to retain this material (e.g. Borrione and Schlitzer, 2013). Taking a bloom abundance of 200 cells mL^{-1}, this requires an accumulated TA uptake of 0.2 μmol kg^{-1} in this area (at 0.5 pmol calcite-C E. hux. cell^{-1} × 200 cells mL^{-1} = 0.1 μmol-C kg^{-1}; two moles of TA are taken per mol of DIC during calcification giving 0.2 μmol kg^{-1} of TA; Ziveri et al., 2000), which does not nearly account for the high ΔTA_{ca} (up to 40 μmol kg^{-1}), even if multiple preceding similar blooms successively grew, calcified and then sedimented out. Advection of lower TA waters from north of the Polar Front through eddies (Meredith et al., 2003) followed by mixing could also cause a TA decrease in this area, which would necessarily be included in the calculation of the ΔTA_{ca} component in case the eddies did not influence the WW layer.

In the regions strongly affected by freshwater inputs – adjacent to South Georgia and where sea-ice had recently retreated – ΔTA_{ca} took negative values relative to net ΔTA. This can possibly be explained by calcium carbonate dissolution occurring in these regions. Dissolution of ikaite crystals during sea-ice melt (Dieckmann et al., 2008) could have contributed TA to the surface waters. The freshwater that was supplied hence did not have zero TA, contrary to the assumption that was made in the calculation of the ΔTA_{fw} component (Friis et al., 2003). Glacial freshwater inputs in the vicinity of South Georgia are likely to have enhanced TA, thereby contributing to the observed 'dissolution' signal.

5.1.3. ΔDIC_{resid}

Finally, the ΔDIC_{resid} was calculated from the net ΔDIC and its components that have been discussed. The sum of the ΔDIC_{fw}, ΔDIC_{bio} and ΔDIC_{ca} was typically greater than net ΔDIC, leading to ΔDIC_{resid} taking negative values as a fraction of net ΔDIC (Fig. 6i). This means that there was mostly a net uptake of atmospheric CO_2 by the ocean, by direct air-sea gas exchange, from winter to summer. The strongest negative ΔDIC_{resid}, relative to net ΔDIC, was found in the South Georgia and South Sandwich Islands bloom, and this was dominantly driven by the very high ΔDIC_{bio} in those areas which was stimulated by shelf derived iron inputs; primary productivity is therefore a key control on air-sea CO_2 exchange and seawater carbonate chemistry in this region, as previously reported (Bakker et al., 2008). Values of ΔDIC_{resid} close to zero were observed in the areas that had recently experienced sea-ice retreat such as the Weddell Sea; here, the net winter-to-summer change in DIC was effectively entirely accounted for by the freshwater input (Fig. 6a), and there was not any significant primary productivity. As mentioned in the previous section, it appears ikaite may have been present in the sea-ice in the Weddell Sea, contributing TA and DIC to surface waters upon sea-ice melt (1 DIC: 2 TA; Wolf-Gladrow et al., 2007). The assumption of a zero end member for DIC results in an overestimation of the freshwater component, $\Delta DIC_{fw,}$ and an underestimation of the residual. However the contribution from ikaite was very small (Fig. 6h) and did not affect the calculation of the residual term. The physical and biogeochemical processes controlling carbonate chemistry in sea-ice influenced area are discussed further in Section 5.4.

Integration of ΔDIC_{resid} over the depth of the mixed layer observed at the Southern Ocean sampling stations reveals an increased dominance of the South Georgia and South Sandwich Islands blooms for atmospheric CO_2 uptake (Fig. S9). It is important to first note that this result is sensitive to the mixed layer depth, and this calculation depends on the mixed layer depths observed during a single cruise. In case they are not representative of typical conditions, then this integrated value will also be erroneous. Nevertheless, if we assume that the ΔDIC_{resid} is evenly distributed through the mixed layer, we find net seasonal air-to-sea CO_2 fluxes of up to -50 g-C m^{-2} in these bloom areas. This is consistent with CO_2 flux estimates for this region based on a global climatology of pCO_2^{sw} measurements (Takahashi et al., 2009). Our observations also indicate that the Scotia Sea was overall a sink of CO_2 with net seasonal air-to-sea CO_2 fluxes of up to ca. -12 g-C m^{-2} in agreement with a report by Schlitzer (2002), with areas in the central region acting as a source, in agreement with austral summer observations by (Jones et al., 2012) (Fig. S9).

5.1.4. *ΔpH and $\Delta\Omega_{ar}$*

The high pH and Ω_{ar} values in the vicinity of South Georgia corresponded to areas with a strong uptake of DIC due to primary production (ΔDIC^{bio}), which considerably increased pH (ΔpH^{bio} 0.35–0.55) and Ω_{ar} ($\Delta\Omega_{ar}{}^{bio}$ 0.8–1.3) (Fig. 7). While the decrease in DIC and TA in this area attributed to calcium carbonate production (which also includes advection effects as discussed previously) also decreased pH (ΔpH^{ca} -0.02 to -0.06) and Ω_{ar} ($\Delta\Omega_{ar}{}^{ca}$ -0.1 to -0.3), the comparatively larger organic carbon production counteracted this and resulted in enhanced pH (8.2–8.3) and Ω_{ar} (2.2–2.6) values north of South Georgia. In the waters immediately north of South Georgia, low pH (7.9–8.1) and Ω_{ar} (1.2–1.6) corresponded to areas where the calcium carbonate term was negative ($\Delta\Omega_{ar}{}^{ca} - 0.2$), but biological production was relatively low ($\Delta\Omega_{ar}{}^{bio} < 0.4$) compared with the region further north of South Georgia. Southwards advection, through eddy formation, of waters with decreased pH and Ω_{ar} from north of the polar front (lower TA) to the region directly north of South Georgia, is a possible supply mechanism. These processes resulted in an area north of South Georgia with strong horizontal gradients (pH 7.9–8.3 and Ω_{ar} 1.2–2.6).

Freshwater inputs had only minor effects on pH ($\Delta pH^{fw} < 0.008$) and these were limited to the southern areas where sea-ice had melted, or to the glacial runoff close to South Georgia. A similar pattern was observed for the calcium carbonate saturation state but with larger effects ($\Delta\Omega_{ar}{}^{fw}$ up to -0.06). Variations in pH and Ω_{ar} due to sea-ice melt are discussed in detail in Section 5.4.

5.2. Spatial variations in the Arctic

In contrast to the Southern Ocean, our study area in the Arctic does not experience the temperature inversion that allows the calculation of winter water values and a seasonal evaluation of carbonate chemistry controls. Here we use horizontal variations in surface carbonate chemistry in combination with upper water column data to elucidate the processes that drive the surface gradients in pH and Ω_{ar}. The upper water column in the Arctic showed strong gradients in both TA and DIC (Fig. S10) resulting from the presence of different water masses and sea ice across the Norwegian and Greenland Seas (Skjelvan et al., 1999), moving from warm, salty Atlantic waters to cold, ice-covered Polar waters. In addition, the strong gradients in carbonate chemistry variables in the Fram Strait, highlighted the role of advection in this area, where strong stratification prevents vertical mixing (Blindheim and Østerhus, 2005). The surface gradients in pH and Ω_{ar} are equally as sharp and appear to correlate with temperature and salinity changes (Fig. 4), particularly in the polar water influenced Greenland Sea and Fram Strait, suggesting that the physical processes controlling water mass composition largely determined surface pH and Ω_{ar} in these regions.

Interestingly, a decoupling between pH and Ω_{ar} was observed over strong temperature and salinity gradients in waters featuring low productivity (Fig. S4), both in the northern part of the Barents Sea transect and in the Denmark Strait. In these regions, the salinity derived TA and DIC decreases (Fig. 2) coincided with a temperature decrease from 6 to 0 °C (Fig. 4). In the northern Barents Sea, for example, the pH increased relative to the south (Fig. 4) due to the temperature decrease (sensitivity is ca. 0.0114 pH $°C^{-1}$; Gieskes, 1969), with $pH_{T=6}$ ca. 8.15 and $pH_{T=0}$ ca. 8.25. However, Ω_{ar} did not show a similar increase (Fig. 4) due to the much smaller temperature sensitivity (0.001 $°C^{-1}$), and since both TA and DIC were reduced in equal proportion, Ω_{ar} was only slightly lower as a result of the lower calcium ion concentrations in the fresher waters.

Elevated surface pH and Ω_{ar} values along the ice edge corresponded to lower nitrate concentrations indicating biological CO_2 uptake (Fig. 4). Abundant iron (Fig. S8) and high chl-*a* concentrations (Fig. S11) corresponded to low DIC (Fig. 2) providing further evidence for the effect of autotrophy on surface pH and Ω_{ar}. Indeed, during the Arctic cruise phytoplankton blooms were observed along the sea-ice edge, over shallow shelves and in coastal areas as confirmed by chl-*a* concentrations (Fig. S11). The surface dissolved iron concentrations in the Arctic region were high compared to the Southern Ocean (Fig. S8), with only 3 out of 125 datapoints falling under 0.2 nM (south of Jan Mayen), indicating that iron limitation of primary productivity was not likely in this study region. Enhanced dissolved iron levels for the Arctic Ocean have also been reported by Klunder et al. (2012) mainly attributed to benthic supply in the shelf regions. The strong influence of biological CO_2 uptake on pH and Ω_{ar} is clearly illustrated by maxima near Jan Mayen (e.g. pH from 8.15 to 8.35 and Ω_{ar} from 2 to 2.9) (Fig. 4), in the southern Norwegian Sea close to Iceland, along the Norwegian Coast and around Svalbard, coinciding with reduced DIC and enhanced chlorophyll concentrations (Figs. 2a and S7). Enhanced iron inputs from Svalbard are evident in its coastal waters (Fig. S8), stimulating phytoplankton bloom development (as observed in satellite data at 76 °N 20 °E (Fig. S11)), nutrient uptake and increased pH and Ω_{ar} (Fig. 4, 1500 nautical miles along cruise route). A previous analysis over a full annual cycle in the Barents Sea Opening also showed the large impact of biological activity on Ω_{ar}, for 45–70% of the difference between winter and summer values (Tynan et al., 2014).

5.3. Principal component analysis (PCA)

PCA was applied to allow visualisation of the relationships between the environmental forcing variables (Fig. S4) and showed different forcing factors on each of the components for the two polar regions (Table 2). DIC, nitrate, phosphate and calcium carbonate saturation states determined PC1 in both the Arctic and Southern Ocean. This component was taken as an indicator of biological activity. PC2 was influenced by temperature, salinity and TA in the Arctic, but by temperature, TA and silicate in the Southern Ocean. This component was taken as an indicator of water masses. For the Arctic, PC1 explained 44.1% of the variation whilst PC2 captured 26.7% of the variation. For the Southern Ocean, PC1 explained 38.8% of the variation whilst PC2 captured 32.6% of the variation. The relative variations of the two principal components along the cruise sections (Fig. 8) indicate a strong coupling between physical processes and biological activity in the Arctic, while this was not the case for our transect in the Southern Ocean. In the Arctic, the identified principal components varied almost identically (Fig. 8), i.e. a change in the biological signal was accompanied by a change in water masses. This is consistent with the strong correlation of gradients in pH and Ω_{ar} with temperature

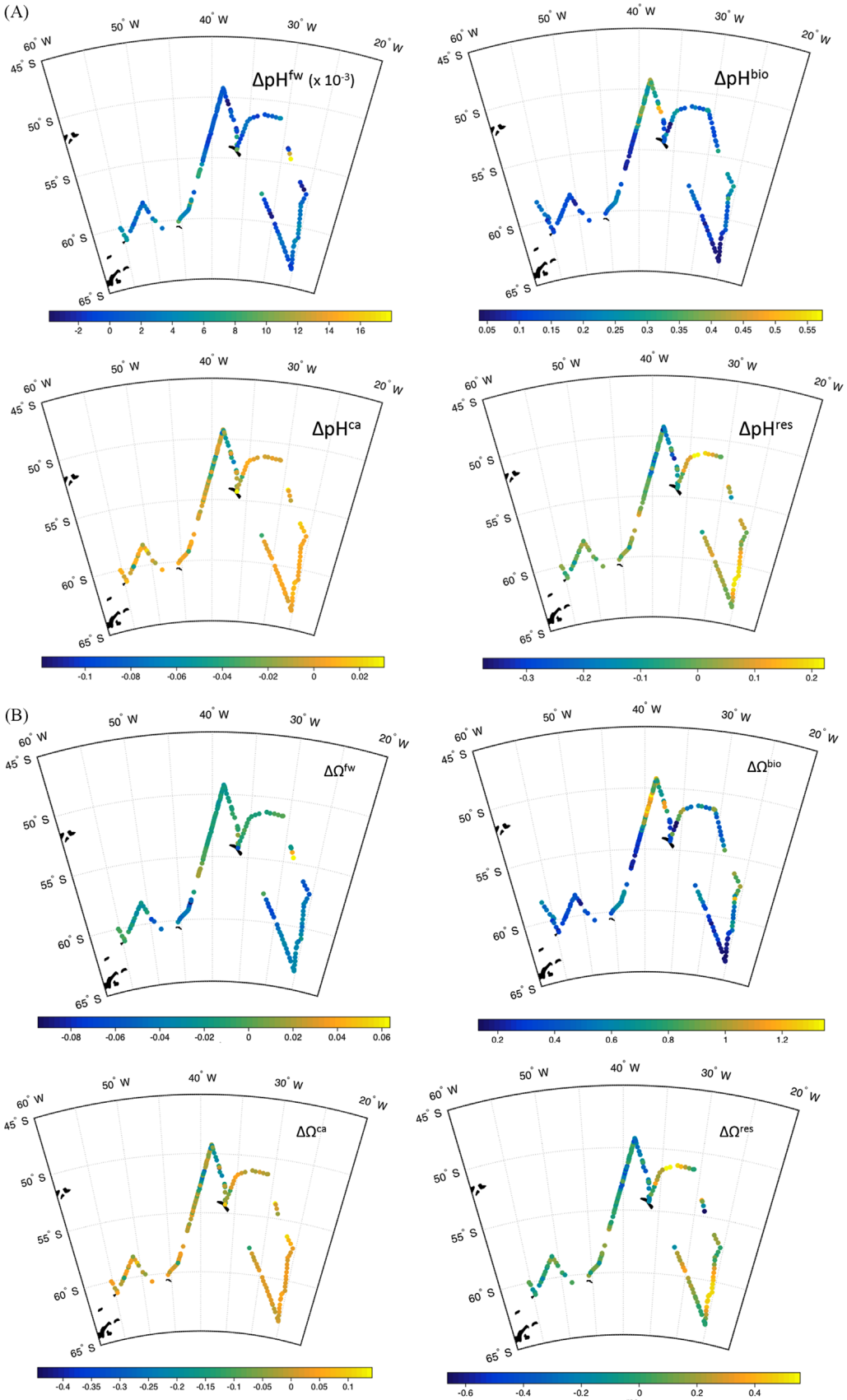

Fig. 7. Components of the net seasonal changes in (a) pH and (b) Ω_{ar} as determined by analysis of the WW layer (Sections 3.4 and 5.1). Components are fw=freshwater, bio=biological, ca=calcification, and resid=residual (i.e. physical processes), as discussed in the text.

Table 2
Principal component analysis (PCA) loadings.

	Arctic		S. Ocean	
Variable	PC1	PC2	PC1	PC2
Salinity	0.21	**0.52**	−0.10	0.35
Temperature	−0.05	**0.44**	0.02	**0.52**
Nitrate	**0.45**	−0.06	−**0.36**	−0.30
Phosphate	**0.42**	−0.09	−**0.41**	−0.21
Silicate	0.23	−0.03	0.03	−**0.49**
TA	0.18	**0.55**	0.18	−**0.39**
DIC	**0.42**	0.23	−**0.46**	−0.12
Calcite saturation	−**0.38**	0.29	**0.47**	−0.21
Aragonite saturation	−**0.38**	0.30	**0.47**	−0.14
Iron	−0.11	−0.05	−0.08	0.13
(*n*)	84		64	

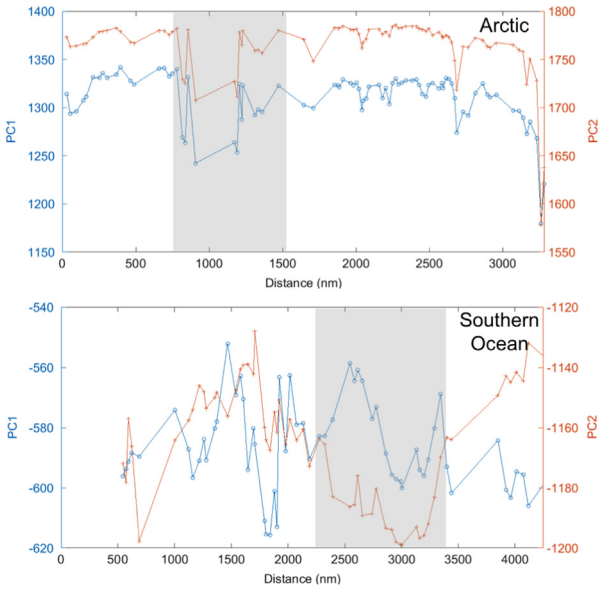

Fig. 8. Principal component variations in the Arctic and Southern Ocean. Grey shaded areas are the sea-ice influenced areas in the Fram Strait (Arctic) and Weddell Sea (Southern Ocean).

and salinity as discussed above. In the Southern Ocean, the principal components did not follow such a clear trend, most times displaying opposite trajectories (Fig. 8). This indicates that biological activity did not always correlate with a change in water masses, as discussed above for South Georgia and the South Sandwich Islands, where iron supply stimulated biological activity in the otherwise HNLC Southern Ocean.

5.4. Sea ice influenced areas

Different physical and biogeochemical processes controlled the carbonate system following sea-ice melt in the Fram Strait and Weddell Sea. Temperature forms an important control on pH changes (ca. 0.0114 pH °C^{-1}; Gieskes, 1969), however the strong pH gradients in the Fram Strait (from pH 8.05 to 8.45) far exceeded the pH change caused by temperature alone (6 °C) (assuming the absence of atmospheric CO_2 uptake caused by cooling of the surface ocean). Additionally, the lowest pH values (8.00–8.10) were observed in the areas with coldest waters (ca. −1.3 °C), and corresponded with low Ω_{ar} values (1.1–1.4) suggesting organic matter respiration determined these variations.

TA and DIC in the Arctic region showed large gradients but they each had different relationship with salinity (Fig. 9). TA changes

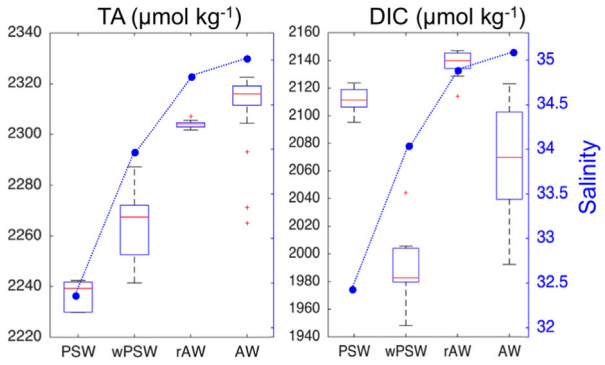

Fig. 9. Average salinity, total alkalinity (TA) and dissolved inorganic carbon (DIC) concentrations for water masses in the Fram Strait (PSW: Polar Surface water; wPSW: warm Polar Surface Water; AW: Atlantic Water; rAW: recirculated Atlantic Water); The red line is the median, the edges of the box are the 25th and 75th percentiles, and the whiskers show the range of values not considered outliers. (For interpretation of the references to colour in this figure legend, the reader is referred to the web version of this article.)

corresponded largely with salinity, decreasing from the salty Atlantic waters further east to the fresher Polar waters further west (Fig. 9). A similar trend was not evident for DIC (Fig. 9). The low DIC concentrations in the warm PSW on the ice-edge corresponded to a pronounced phytoplankton bloom, supported by satellite chl-*a* (Fig. S11). Summer blooms are known to cause strong drawdown of DIC in this region (Miller et al., 1999). The high DIC concentrations in PSW (Fig. 9) were observed in waters below thick ice (ca. 80% cover, Fig. 1), indicating accumulated DIC under the ice.

Apparent oxygen utilisation (AOU) can be used to derive biological activity as oxygen is produced (consumed) on photosynthesis (respiration). Air-sea oxygen equilibration times can be relatively quick (Broecker and Peng, 1974) and therefore AOU may not fully reflect biological activity in areas which have recently been in contact with the atmosphere. The waters in the western side of the Fram Strait were under ice and are assumed to have been covered since the previous winter as these waters come from regions further upstream in the Arctic Ocean. Although gas exchange with the atmosphere can occur through sea-ice (Crabeck et al., 2014; Zhou et al., 2013) this is not well constrained and for the purposes of our study we assume air-sea exchange was limited under ice.

Water column pH and Ω_{ar} showed two divergent profiles in the Fram Strait: in open waters, surface pH and Ω_{ar} values were higher with respect to subsurface waters, while in ice-covered stations they were lower (Fig. 10a). AOU correlated negatively with pH and Ω_{ar}, with higher surface pH and Ω_{ar} in productive waters (AOU < 0) and lower where respiration was apparent (AOU > 0) (Fig. 10a). A pronounced sea-ice edge bloom (8 mg m^{-3} chlorophyll-*a* estimated from Fig. S11a) resulted in low DIC concentrations (Fig. 9 and S12; ca. 1980 μmol kg^{-1}) due to biological uptake, with consequent enhanced $\delta^{13}C_{DIC}$ (2.5‰, Fig. S12) due to preferential uptake of light $\delta^{13}C$ by photosynthesising autotrophs (Quay et al., 2003), and depleted nutrient concentrations (Fig. S12). As a result pH increased by 0.33 and Ω_{ar} by 1.6 with respect to subsurface values (Fig. 10b), as has been observed in other areas of the Arctic Ocean following biological production after sea-ice melt (Bates et al., 2009; Chierici et al., 2011). The surface waters under the ice had a positive AOU (Fig.10b) due to organic matter remineralisation, as also reported by Bates et al (2009) for the western Arctic Ocean, with higher DIC concentrations (Fig. 9; ca. 2110 μmol kg^{-1}) suggesting respired CO_2 is responsible for lowering the pH (−0.05) and Ω_{ar} (−0.3) (Fig. 10b). This respiration signal is considered to be derived from degradation of organic

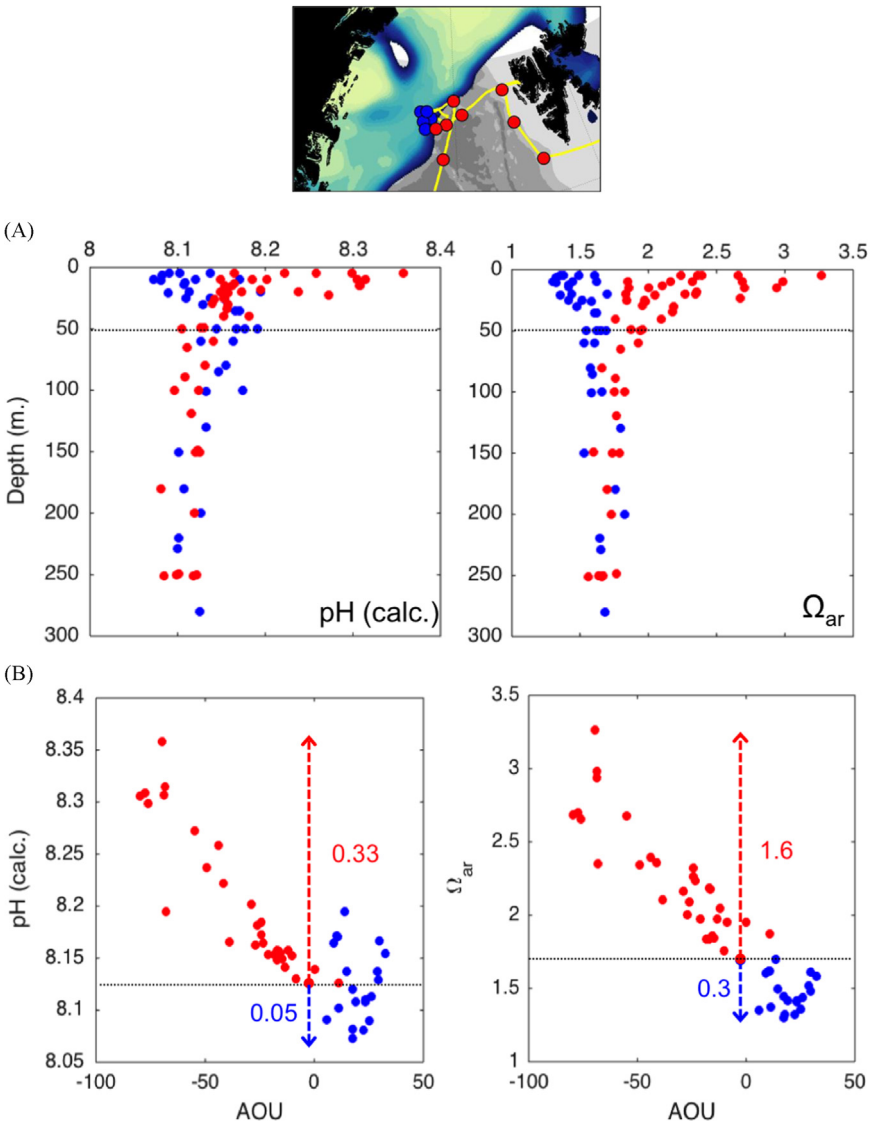

Fig. 10. (a) Water column profiles of pH and Ω_{ar} in the Fram Strait. The upper water column (< 50 m) is marked with a dashed grey line. (b) Upper water column (< 50 m) variability of pH and Ω_{ar} against apparent oxygen utilisation (AOU). Dashed grey line marks the average pH and Ω_{ar} below 50 m. Red (blue) dots correspond to the stations in red (blue) on the map. Shading in upper plot same as Fig. 1, with cruise track marked in yellow. (For interpretation of the references to colour in this figure legend, the reader is referred to the web version of this article.)

matter upstream in the Arctic Ocean (Skoog et al., 2001), which accumulates in surface waters under the ice and is transported to the Fram Strait. This is also evident in the $\delta^{13}C_{DIC}$ observations with the high DIC concentrations (ca. 2120 µmol kg^{-1}) matching reduced $\delta^{13}C_{DIC}$ (ca. 1.0‰) due to remineralisation of biological debris with light $\delta^{13}C$ signatures and comparatively larger DIN concentrations (ca. 6 µmol kg^{-1}) (Fig. S12).

In contrast, in the Weddell Sea, temperature and salinity variations were minor (Fig. 5), and mainly the result of recent sea-ice melt over the most southern area (Fig. S6 indicates the sea-ice fraction one month prior to the cruise). However, pronounced horizontal gradients in pH (from 8.30 to 8.10) and Ω_{ar} (from 2.4 to 1.6) were observed (Fig. 5) with minor changes in water mass properties (ΔT 1 °C and ΔS 0.4; Fig. 5). We use the seasonal drawdown described in Section 5.1, to explain these gradients.

While pH and Ω_{ar} increased from winter to summer across the Weddell Sea, regional differences were evident (Fig. 11a). In the vicinity of the South Sandwich Islands, a large increase in pH (0.25) and Ω_{ar} (2.1) (Fig. 11a) corresponded to a large decrease in DIN concentrations (as much as 16 µmol kg^{-1}; Fig. 11a) attributed primarily to the biological component (ΔDIN^{bio}, Fig. 6d). Increased shelf-derived iron inputs from the islands (concentrations up to 0.45 nM; Fig. 11b) facilitated a bloom after sea-ice retreat (Fig. S7a; Cavan et al. 2015) and the uptake of DIN and DIC (Fig. 6e). This is in agreement with previous reports of enhanced biological activity in the Weddell Sea (Hewes et al., 2008), and the strong control by biological activity on seasonal DIC variations (Jones et al., 2010). The biological activity resulted in dFe uptake, such that dFe concentrations in the vicinity of the South Sandwich Islands (region between ca. 2700 and 2800 nm) had been depleted (Fig. 11c) whilst pH and Ω_{ar} values were enhanced (Fig. 11a and b). In contrast, in regions beyond 2800 nm with low iron concentrations (< 0.2 nM; Fig. 11b), no bloom was observed (Fig. S7), despite stratification and increased light availability after sea ice melt. The depth of the mixed layer determines bloom initiation (Nelson and Smith Jr., 1991), however this depth was constant across the Weddell Sea (ca. 30 m, Fig. S13) and therefore bloom formation in this case was determined by iron availability. Mattsdotter Björk et al. (2014) found that sea-ice melt in the Ross Sea supplied enough iron, and together with enhanced stratification, promoted

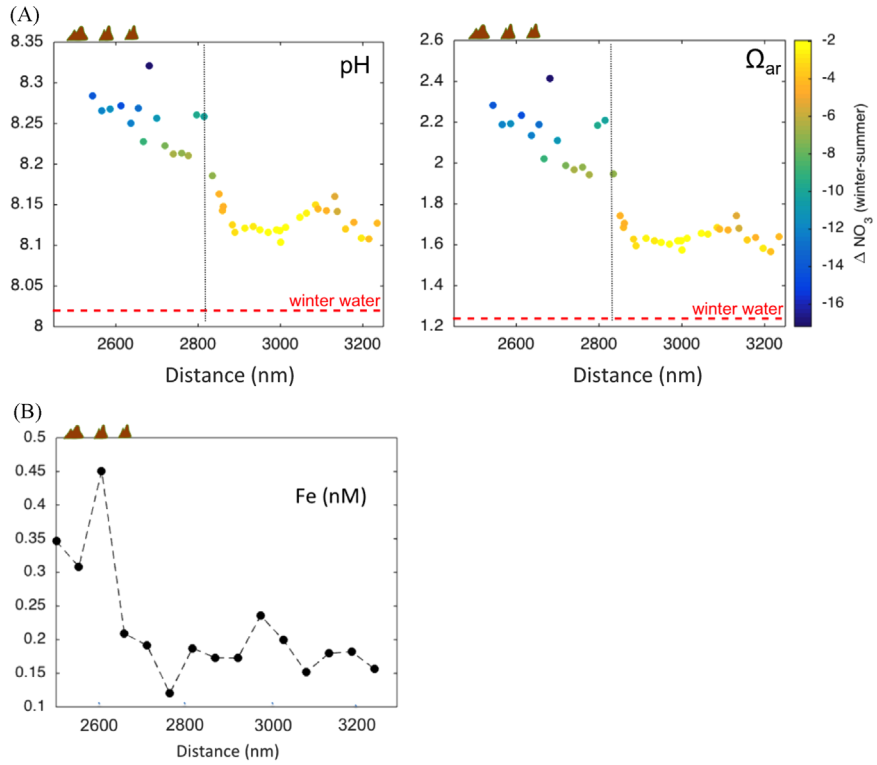

Fig. 11. (a) Surface pH and Ω_{ar} in the Weddell Sea. Colours represent changes in surface nitrate concentrations from winter to summer. The dashed red line represents average winter water values for pH and Ω_{ar}, respectively. The dotted grey line divides the Fe-fertilised from the non-Fe fertilised region (b) Surface dissolved iron concentrations in the Weddell Sea. The South Sandwich Islands are shown on top left of graphs for reference. (For interpretation of the references to colour in this figure legend, the reader is referred to the web version of this article.)

an ice-edge bloom resulting in high pH (8.3) and Ω_{ar} (1.8) values. The difference in iron concentrations in Antarctic sea-ice can be explained by the variability of iron supply at the time of sea-ice formation (Lannuzel et al., 2010).

Overall, pH and Ω_{ar} in the naturally iron-fertilised region around the South Sandwich Islands increased over three times as much as in the non-fertilised area in the Weddell Sea (Fig. 12). The effect of freshwater inputs was negligible on pH and Ω_{ar}, while temperature slightly decreased pH, as expected from the warming of surface waters from winter to summer (Fig. 12). Biological activity was the largest factor contributing to the increase in pH and Ω_{ar} across the Weddell Sea (55–65%; Fig. 12). The residual indicated an increase in pH and $\Omega_{ar,}$ and was larger in the iron-fertilised area than in the non-fertilised area (Fig. 12). The residual represents physical processes (air-sea gas exchange, mixing, upwelling, and advection) plus a disequilibrium term, unaccounted for by the other terms. However sources of error in the biological term, for example from the use of an inaccurate C:N ratio, could result in an unaccounted biological impact, which would be carried in the residual. If this is the case, areas with higher biological activity would necessarily have larger residuals. Spatiotemporal deviations from the Redfield ratio occur due to species composition (Martiny et al., 2013) and stage of the bloom (Sambrotto et al., 1993). The C:N ratio in the South Sandwich Island bloom may have been higher than Redfield as observed in other areas of the Southern Ocean (Arrigo et al., 1999), underestimating the drawdown in DIC (DIC^{bio}) subsequently used to calculate the biological impact on pH and Ω_{ar}, and producing a larger residual in the iron fertilised area (Fig. 12).

6. Synthesis and conclusions

Horizontal gradients in surface pH and Ω_{ar} in the Arctic and Southern Ocean were due to the prevalence of different physical and biogeochemical processes in each ocean (Fig. 13). In the Arctic, variations in water mass temperature and salinity determined pH and Ω_{ar} through changes in TA, while biology did so primarily by forcing DIC changes. In the Southern Ocean, variations in salinity controlled pH and Ω_{ar} (through changes in TA) but these variations were small, and larger changes in TA arising from a combination of calcification, advection and upwelling, had a more pronounced impact on pH and Ω_{ar}. While biological activity in the HNLC Southern Ocean was limited, a large impact on pH and Ω_{ar} (through DIC drawdown) was observed in regions with enhanced iron supply, including the region north of South Georgia.

The major contrasts between the ice-covered areas in the Southern Ocean and the Arctic can be attributed to differences in biological activity related to iron availability. In the HNLC Southern Ocean, sea-ice retreat only resulted in pronounced blooms and DIC uptake in regions with enhanced iron supply. In the Arctic in contrast, iron was replete, which facilitated bloom development along the ice edge, where nutrient and/or light availability may control productivity. Therefore, the Fram Strait is almost invariably a sink for CO_2 upon ice retreat, while the formation of a CO_2 sink in the Weddell Sea ultimately depends on iron availability.

The increasing marginal ice-zone in the Arctic Ocean (Strong and Rigor, 2013) may favour the formation of more frequent ice-edge blooms in light-limited areas such as the Fram Strait, temporarily increasing saturation states and pH. In contrast, ice-edge blooms do not always form at the marginal ice-zone in the Southern Ocean (Savidge et al., 1996) since both iron and light co-limit primary production (Lancelot et al., 2000). The mass island effect of the South Sandwich Islands should continue to promote bloom formations after a potential future sea-ice retreat in this area, with the associated increase in pH and saturation states in downstream waters. Iron inputs from increased calving of glaciers can lead to local blooms in the HNLC Southern Ocean (Biddle et al.,

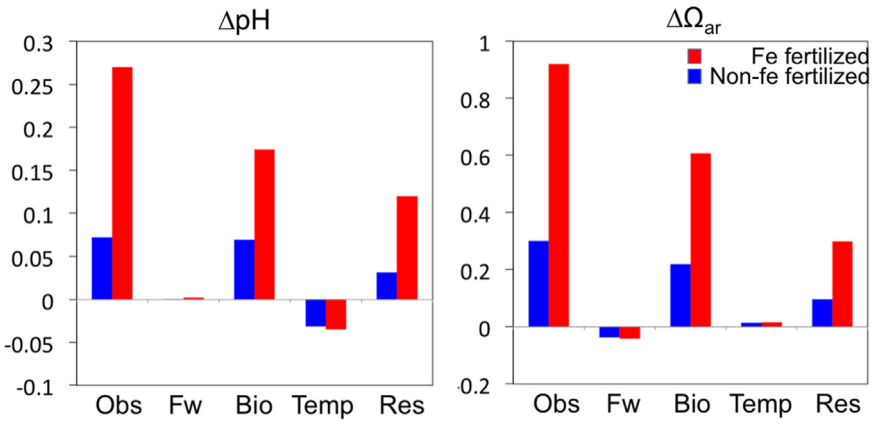

Fig. 12. Changes in pH and Ω_{ar} in the Weddell Sea for the iron fertilised region of the South Sandwich Islands (red) and the non-fertilised region in the Weddell Sea gyre (blue). Changes correspond to the difference between winter water layer and surface waters. [Obs=total observed deficits; Fw=changes due to freshwater inputs; Bio=changes from biological activity; Temp=thermodynamic changes; Res=residual]. (For interpretation of the references to colour in this figure legend, the reader is referred to the web version of this article.)

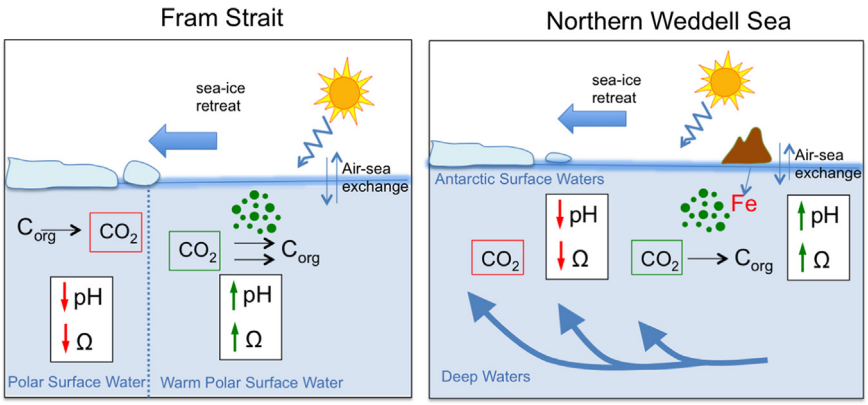

Fig. 13. Representation of the processes controlling pH and Ω distributions in the ice influenced areas in the Arctic (Fram Strait) and the Southern Ocean (Weddell Sea).

2015; Shadwick et al., 2013a) and could potentially increase pH and saturation state in areas of the Weddell Sea further away from the continent. These increases in both the Fram Strait and Weddell Sea can provide some temporal relief for organisms, from the expected global decrease in pH and saturation states due to anthropogenic CO_2 uptake.

The Arctic Ocean has been postulated to be more vulnerable than the Southern Ocean to ocean acidification, due to lower alkalinity and a less pronounced seasonal cycle, which prevents large increases in pH and Ω (Shadwick et al., 2013b). In our areas of study, the Arctic had in general higher pH and Ω_{ar} than the Southern Ocean, suggesting this is not always the case. Shadwick et al. (2013b) pointed out their study is not representative of the Barents Sea and Atlantic inflow areas in the Arctic (as in this study), and indeed, we have previously reported large seasonal increases in Ω_{ar} in the Barents Sea Opening due to biological activity (Tynan et al., 2014). In the present study, we also found very high pH and Ω_{ar} due to primary production in areas close to the ice-edge in the Arctic. These studies suggest that the response of the carbonate system to anthropogenic forcing will not only vary between the two polar oceans but also across them.

Finally, this study provided a carbonate chemistry framework for the biological and biogeochemical variables measured during the UKOA cruises and as such, it highlights the large variability of pH and $\Omega_{ar.}$ to which polar ecosystems may be exposed. Pronounced gradients over small spatial scales may mean that organisms thriving in favourable conditions (high pH and Ω_{ar}) can easily become exposed to lower pH and $\Omega_{ar.}$ This may have detrimental effects on, for example, calcifying organisms with insufficient protective mechanisms. Alternatively, it may be the case that polar ecosystems have adapted to the large variations in pH and Ω_{ar} and are therefore more resilient to anthropogenic ocean acidification.

Acknowledgements

We strongly appreciate the support by the staff involved in the UKOA cruises: the Masters Graham Chapman and Jerry Burgan, officers and crew of the RRS *James Clark Ross* the scientists and technical support staff, particularly Gianna Battaglia and Maxi Castrillejo Iridoy for the iron measurements; the staff of the British Antarctic Survey, Cambridge, National Marine Facilities, Southampton, and the Scottish Association for Marine Science, Oban. We are grateful to the Danish, Icelandic and Norwegian diplomatic authorities for granting permission to travel and work in Greenland, Iceland and Svalbard coastal and offshore waters during the Arctic cruise. We would like to thank the UK Natural Environment Research Council (NERC), the UK Department of Environment, Food and Rural Affairs (DEFRA), and the UK Department of Energy and Climate Change (DECC) for funding the research cruises via the pelagic consortium of UK Ocean Acidification Research Programme (Grant no. NE/H017348/1) and the UK Carbonate Chemistry Facility (Grant no. NE/H025839/1). The OSTIA data were obtained from www.myocean.eu. The altimeter products were produced by Ssalto/Duacs and distributed by Aviso, with support from Cnes (http://www.aviso.altimetry.fr/duacs/).

All data from cruises JR271 and JR274 have been deposited at the British Oceanographic Data Centre (BODC).

Appendix A. Supplementary material

Supplementary data associated with this article can be found in the online version at http://dx.doi.org/10.1016/j.dsr2.2016.01.001.

References

Achterberg, E.P., Holland, T.W., Bowie, A.R., Mantoura, R.F.C., Worsfold, P.J., 2001. Determination of iron in seawater. Anal. Chim. Acta 442, 1–14. http://dx.doi.org/10.1016/S0003-2670(01)01091-1.

Ackley, S.F., 1981. A review of sea-ice weather relationships in the Southern Hemisphere. In: Sea Level, Ice Climate Change: Proceedings of the Canberra Symposium.

Anderson, L.A., Sarmiento, J.L., 1994. Redfield ratios of remineralization determined by nutrient data analysis. Glob. Biogeochem. Cycles 8, 65–80. http://dx.doi.org/10.1029/93GB03318.

Anderson, L., Dyrssen, D., 1981. Chemical constituents of the Arctic Ocean in the Svalbard Area. Oceanol. Acta 4, 305–311.

Arrigo, K.R., Robinson, D.H., Worthen, D.L., Dunbar, R.B., DiTullio, G.R., VanWoert, M., Lizotte, M.P., 1999. Phytoplankton community structure and the drawdown of nutrients and CO_2 in the Southern Ocean. Science 283, 365–367. http://dx.doi.org/10.1126/science.283.5400.365.

Azetsu-Scott, K., Clarke, A., Falkner, K., Hamilton, J., Jones, E.P., Lee, C., Petrie, B., Prinsenberg, S., Starr, M., Yeats, P., 2010. Calcium carbonate saturation states in the waters of the Canadian Arctic Archipelago and the Labrador Sea. J. Geophys. Res. 115, 1–18. http://dx.doi.org/10.1029/2009JC005917.

Azetsu-Scott, K., Starr, M., Mei, Z.-P., Granskog, M., 2014. Low calcium carbonate saturation state in an Arctic inland sea having large and varying fluvial inputs: the Hudson Bay system. J. Geophys. Res. Oceans 119, 6210–6220. http://dx.doi.org/10.1002/2014JC009948.

Bakker, D.C.E., Hoppema, M., Schröder, M., Geibert, W., de Baar, H.J.W., 2008. A rapid transition from ice covered CO_2–rich waters to a biologically mediated CO_2 sink in the eastern Weddell Gyre. Biogeosciences 5, 1373–1386. http://dx.doi.org/10.5194/bg-5-1373-2008.

Bates, N.R., Mathis, J.T., Cooper, L.W., 2009. Ocean acidification and biologically induced seasonality of carbonate mineral saturation states in the western Arctic Ocean. J. Geophys. Res. -Oceans 114, C11007. http://dx.doi.org/10.1029/2008jc004862.

Bednaršek, N., Tarling, G.A., Bakker, D.C.E., Fielding, S., Jones, E.M., Venables, H.J., Ward, P., Kuzirian, A., Lézé, B., Feely, R.A., Murphy, E.J., 2012. Extensive dissolution of live pteropods in the Southern Ocean. Nat. Geosci. 5, 881–885. http://dx.doi.org/10.1038/ngeo1635.

Bellerby, R.G.J., Olsen, A., Furevik, T., Anderson, L.G., 2005. Response of the surface ocean CO_2 system in the Nordic Seas and Northern North Atlantic to climate change. In: Drange, H., Dokken, T., Furevik, T., Gerdes, R., Berger, W. (Eds.), The Nordic Seas: An Integrated Perspective. American Geophysical Union, pp. 189–197.

Biddle, L.C., Kaiser, J., Heywood, K.J., Thompson, A.F., Jenkins, A., 2015. Ocean glider observations of iceberg-enhanced biological production in the northwestern Weddell Sea. Geophys. Res. Lett. 42. http://dx.doi.org/10.1002/2014GL062850.

Blindheim, J., Østerhus, S., 2005. The Nordic Seas, main oceanographic features. In: Helgeange, Dokken, T., Furevik, T., Gerdes, R., Berger, W. (Eds.), The Nordic Seas: An Integrated Perspective. American Geophysical Union, pp. 11–37.

Borrione, I., Schlitzer, R., 2013. Distribution and recurrence of phytoplankton blooms around South Georgia, Southern Ocean. Biogeosciences 10, 217–231. http://dx.doi.org/10.5194/bg-10-217-2013.

Bourke, R.H., Paquette, R.G., Blythe, R.F., 1992. The Jan Mayen current of the Greenland Sea. J. Geophys. Res. Oceans 97, 7241–7250. http://dx.doi.org/10.1029/92JC00150.

Bourke, R.H., Weigel, A.M., Paquette, R.G., 1988. The westward turning branch of the West Spitsbergen Current. J. Geophys. Res. Oceans 93, 14065–14077. http://dx.doi.org/10.1029/JC093iC11p14065.

Bradshaw, A.L., Brewer, P.G., Shafer, D.K., Williams, R.T., 1981. Measurements of total carbon dioxide and alkalinity by potentiometric titration in the GEOSECS program. Earth Planet. Sci. Lett. 55, 99–115. http://dx.doi.org/10.1016/0012-821X(81)90090-X.

Broecker, W.S., Peng, T.-H., 1974. Gas exchange rates between air and sea1. Tellus 26, 21–35. http://dx.doi.org/10.1111/j.2153-3490.1974.tb01948.x.

Caldeira, K., Wickett, M.E., 2003. Oceanography: anthropogenic carbon and ocean pH. Nature 425. http://dx.doi.org/10.1038/425365a.

Cao, L., Caldeira, K., Jain, A.K., 2007. Effects of carbon dioxide and climate change on ocean acidification and carbonate mineral saturation. Geophys. Res. Lett., 34. http://dx.doi.org/10.1029/2006GL028605.

Carmack, E., Wassmann, P., 2006. Food webs and physical-biological coupling on pan-Arctic shelves: Unifying concepts and comprehensive perspectives. Prog. Oceanogr. 71, 446–477. http://dx.doi.org/10.1016/j.pocean.2006.10.004.

Cavan, E.L., Le Moigne, F.A.C., Poulton, A.J., Tarling, G.A., Ward, P., Daniels, C.J., Fragoso, G.M., Sanders, R.J., 2015. Attenuation of particulate organic carbon flux in the Scotia Sea, Southern Ocean, is controlled by zooplankton fecal pellets. Geophys. Res. Lett. 42. http://dx.doi.org/10.1002/2014GL062744.

Chierici, M., Fransson, A., 2009. Calcium carbonate saturation in the surface water of the Arctic Ocean: undersaturation in freshwater influenced shelves. Biogeosciences 6, 2421–2431.

Chierici, M., Fransson, A., Lansard, B., Miller, L.A., Mucci, A., Shadwick, E., Thomas, H., Tremblay, J.E., Papakyriakou, T.N., 2011. Impact of biogeochemical processes and environmental factors on the calcium carbonate saturation state in the Circumpolar Flaw Lead in the Amundsen Gulf, Arctic Ocean. J. Geophys. Res. 116, C00G09. http://dx.doi.org/10.1029/2011jc007184.

Clarke, K.R., Gorley, R., 2006. PRIMER v6: User Manual/Tutorial, PRIMER-E. Plymouth, UK.

Comeau, S., Gattuso, J.-P., Nisumaa, A.-M., Orr, J., 2012. Impact of aragonite saturation state changes on migratory pteropods. Proc. R. Soc. Lond. B Biol. Sci. 279, 732–738. http://dx.doi.org/10.1098/rspb.2011.0910.

Comiso, J.C., 2011. Large decadal decline of the Arctic multiyear ice cover. J. Clim. 25, 1176–1193. http://dx.doi.org/10.1175/JCLI-D-11-00113.1.

Conrad, C.J., Lovenduski, N.S., 2015. Climate-driven variability in the Southern Ocean carbonate system. J. Clim. 28, 5335–5350. http://dx.doi.org/10.1175/JCLI-D-14-00481.1.

Coplen, T.B., 1995. Reporting of stable hydrogen, carbon, and oxygen isotopic abundances. Geothermics 24, 707–712. http://dx.doi.org/10.1016/0375-6505(95)00024-0.

Cottier, F., Hwang, P., Drysdale, L., 2014. JR271 Physical Oceanography Analysis (Cruise Report). Scotish Association for Marine Science, accessed online at http://www.arcticoacruise.org/?page_id=966.

Crabeck, O., Delille, B., Rysgaard, S., Thomas, D.N., Geilfus, N.-X., Else, B., Tison, J.-L., 2014. First "in situ" determination of gas transport coefficients (DO2, DAr, and DN2) from bulk gas concentration measurements (O_2, N_2, Ar) in natural sea ice. J. Geophys. Res. Oceans 119, 6655–6668. http://dx.doi.org/10.1002/2014JC009849.

De Baar, H.J.W., de Jong, J.T.M., Bakker, D.C.E., Löscher, B.M., Veth, C., Bathmann, U., Smetacek, V., 1995. Importance of iron for plankton blooms and carbon dioxide drawdown in the Southern Ocean. Nature 373, 412–415. http://dx.doi.org/10.1038/373412a0.

Dickson, A.G., 1990a. Thermodynamics of the dissociation of boric acid in synthetic seawater from 273.15 to 318.15 K. Deep-Sea Res. Part Oceanogr. Res. Pap. 37, 755–766. http://dx.doi.org/10.1016/0198-0149(90)90004-F.

Dickson, A.G., 1990b. Standard potential of the reaction: $AgCl(s)+12H_2(g)=Ag(s)+HCl(aq)$, and and the standard acidity constant of the ion HSO_4^- in synthetic sea water from 273.15 to 318.15 K. J. Chem. Thermodyn. 22, 113–127. http://dx.doi.org/10.1016/0021-9614(90)90074-Z.

Dickson, B., Meincke, J., Rhines, P., 2008. Arctic–subarctic ocean fluxes: defining the role of the Northern Seas in climate. In: Dickson, R.R., Meincke, J., Rhines, P. (Eds.), Arctic–Subarctic Ocean Fluxes. Springer, the Netherlands, pp. 1–13.

Dieckmann, G.S., Nehrke, G., Papadimitriou, S., Göttlicher, J., Steininger, R., Kennedy, H., Wolf-Gladrow, D., Thomas, D.N., 2008. Calcium carbonate as ikaite crystals in Antarctic sea ice. Geophys. Res. Lett. 35, L08501. http://dx.doi.org/10.1029/2008GL033540.

Dong, S., Sprintall, J., Gille, S.T., Talley, L., 2008. Southern Ocean mixed-layer depth from Argo float profiles. J. Geophys. Res. Oceans 113, C06013. http://dx.doi.org/10.1029/2006JC004051.

Donlon, C.J., Martin, M., Stark, J., Roberts-Jones, J., Fiedler, E., Wimmer, W., 2012. The Operational Sea Surface Temperature and Sea Ice Analysis (OSTIA) system. Remote Sens. Environ. 116, 140–158. http://dx.doi.org/10.1016/J.Rse.2010.10.017.

Ericson, Y., Ulfsbo, A., van Heuven, S., Kattner, G., Anderson, L.G., 2014. Increasing carbon inventory of the intermediate layers of the Arctic Ocean. J. Geophys. Res. Oceans 119, 2312–2326. http://dx.doi.org/10.1002/2013JC009514.

Evans, W., Mathis, J.T., Cross, J.N., 2014. Calcium carbonate corrosivity in an Alaskan inland sea. Biogeosciences 11, 365–379. http://dx.doi.org/10.5194/bg-11-365-2014.

Fabry, V.J., 2008. Marine calcifiers in a High-CO_2 Ocean. Science 320, 1020–1022. http://dx.doi.org/10.1126/science.1157130.

Falck, E., Anderson, L.G., 2005. The dynamics of the carbon cycle in the surface water of the Norwegian Sea. Mar. Chem. 94, 43–53. http://dx.doi.org/10.1016/j.marchem.2004.08.009.

Findlay, H.S., Tyrrell, T., Bellerby, R.G.J., Merico, A., Skjelvan, I., 2008. Carbon and nutrient mixed layer dynamics in the Norwegian Sea. Biogeosciences 5, 1395–1410.

Fransson, A., Chierici, M., Nojiri, Y., 2009. New insights into the spatial variability of the surface water carbon dioxide in varying sea ice conditions in the Arctic Ocean. Cont. Shelf Res. 29, 1317–1328. http://dx.doi.org/10.1016/j.csr.2009.03.008.

Friis, K., Kortzinger, A., Wallace, D.W.R., 2003. The salinity normalization of marine inorganic carbon chemistry data. Geophys. Res. Lett. 30, 1085. http://dx.doi.org/10.1029/2002GL015898.

Gieskes, J.M., 1969. Effect of temperature on the pH of seawater. Limnol. Oceanogr. 14, 679–685. http://dx.doi.org/10.4319/lo.1969.14.5.0679.

Goyet, C., Poisson, A., 1989. New determination of carbonic acid dissociation constants in seawater as a function of temperature and salinity. Deep-Sea Res. Part Oceanogr. Res. Pap. 36, 1635–1654. http://dx.doi.org/10.1016/0198-0149(89)90064-2.

Hartmann, M., Hill, P.G., Tynan, E., Achterberg, E.P., Leakey, R.J.G., Zubkov, M.V., 2016. Resilience of SAR11 bacteria to rapid acidification in the high-latitude open ocean. FEMS MIcrobiol. Ecol. 92 (2). http://dx.doi.org/10.1093/femsec/fiv161.

Hewes, C.D., Reiss, C.S., Kahru, M., Mitchell, B.G., HolmHansen, O., 2008. Control of phytoplankton biomass by dilution and mixed layer depth in the western

Weddell-Scotia Confluence. Mar. Ecol. Prog. Ser. 366, 15–29. http://dx.doi.org/10.3354/meps07515.
Hinz, D.J., Poulton, A.J., Nielsdóttir, M.C., Steigenberger, S., Korb, R.E., Achterberg, E. P., Bibby, T.S., 2012. Comparative seasonal biogeography of mineralising nannoplankton in the Scotia Sea: *Emiliania huxleyi*, Fragilariopsis spp. and Tetraparma pelagica. Deep-Sea Res. Part II Top. Stud. Oceanogr. 59–60, 57–66. http://dx.doi.org/10.1016/j.dsr2.2011.09.002.
Hopkins, J., Henson, S.A., Painter, S.C., Tyrrell, T., Poulton, A.J., 2015. Phenological characteristics of global coccolithophore blooms. Glob. Biogeochem. Cycles 29. http://dx.doi.org/10.1002/2014GB004919.
Hoppe, C.J.M., Hassler, C.S., Payne, C.D., Tortell, P.D., Rost, B., Trimborn, S., 2013. Iron limitation modulates ocean acidification effects on Southern Ocean Phytoplankton communities. PLoS One 8. http://dx.doi.org/10.1371/journal.pone.0079890.
Humphreys, M.P., Achterberg, E.P., Griffiths, A.M., McDonald, A., Boyce, A.J., 2015. Measurements of the stable carbon isotope composition of dissolved inorganic carbon in the northeastern Atlantic and Nordic Seas during summer 2012. Earth Syst. Sci. Data 7, 127–135. http://dx.doi.org/10.5194/essd-7-127-2015.
Hutchins, D.A., Bruland, K.W., 1998. Iron-limited diatom growth and Si:N uptake ratios in a coastal upwelling regime. Nature 393, 561–564. http://dx.doi.org/10.1038/31203.
Jennings, J.C., Gordon, L.I., Nelson, D.M., 1984. Nutrient depletion indicates high primary productivity in the Weddell Sea. Nature 309, 51–54. http://dx.doi.org/10.1038/309051a0.
Jones, E.M., Bakker, D.C.E., Venables, H.J., Watson, A.J., 2012. Dynamic seasonal cycling of inorganic carbon downstream of South Georgia, Southern Ocean. Deep-Sea Res. Part II Top. Stud. Oceanogr. 59–60, 25–35. http://dx.doi.org/10.1016/j.dsr2.2011.08.001.
Jones, E.M., Bakker, D.C.E., Venables, H.J., Whitehouse, M.J., Korb, R.E., Watson, A.J., 2010. Rapid changes in surface water carbonate chemistry during Antarctic sea ice melt. Tellus Ser. B-Chem. Phys. Meteorol. 62, 621–635. http://dx.doi.org/10.1111/j.1600-0889.2010.00496.x.
Jones, E.P., Anderson, L.G., Jutterström, S., Mintrop, L., Swift, J.H., 2008a. Pacific freshwater, river water and sea ice meltwater across Arctic Ocean basins: results from the 2005 Beringia expedition. J. Geophys. Res. Oceans 113, C08012. http://dx.doi.org/10.1029/2007JC004124.
Jones, E.P., Anderson, L.G., Jutterström, S., Swift, J.H., 2008b. Sources and distribution of fresh water in the East Greenland Current. Prog. Oceanogr. 78, 37–44. http://dx.doi.org/10.1016/j.pocean.2007.06.003.
Kahru, M., Mitchell, B.G., Gille, S.T., Hewes, C.D., Holm-Hansen, O., 2007. Eddies enhance biological production in the Weddell-Scotia Confluence of the Southern Ocean. Geophys. Res. Lett. 34, L14603. http://dx.doi.org/10.1029/2007GL030430.
Kapsenberg, L., Kelley, A.L., Shaw, E.C., Martz, T.R., Hofmann, G.E., 2015. Near-shore Antarctic pH variability has implications for the design of ocean acidification experiments. Sci. Rep. 5. http://dx.doi.org/10.1038/srep09638.
Klunder, M.B., Laan, P., Middag, R., de Baar, H.J.W., Bakker, K., 2012. Dissolved iron in the Arctic Ocean: important role of hydrothermal sources, shelf input and scavenging removal. J. Geophys. Res. Oceans 117, C04014. http://dx.doi.org/10.1029/2011JC007135.
Korb, R.E., Whitehouse, M.J., Atkinson, A., Thorpe, S.E., 2008. Magnitude and maintenance of the phytoplankton bloom at South Georgia: a naturally iron-replete environment. Mar. Ecol. Prog. Ser. 368, 75–91. http://dx.doi.org/10.3354/meps07525.
Korb, R.E., Whitehouse, M.J., Thorpe, S.E., Gordon, M., 2005. Primary production across the Scotia Sea in relation to the physico-chemical environment. J. Mar. Syst. 57, 231–249. http://dx.doi.org/10.1016/j.jmarsys.2005.04.009.
Kostianoy, A.G., Nihoul, J.C.J., 2009. Frontal zones in the Norwegian, Greenland, Barents and Bering Seas. In: Nihoul, J.C.J., Kostianoy, A.G. (Eds.), Influence of Climate Change on the Changing Arctic and Sub-Arctic Conditions, NATO Science for Peace and Security Series C: Environmental Security. Springer, the Netherlands, pp. 171–190.
Kroeker, K.J., Micheli, F., Gambi, M.C., 2013. Ocean acidification causes ecosystem shifts via altered competitive interactions. Nat. Clim. Change 3, 156–159. http://dx.doi.org/10.1038/nclimate1680.
Kvingedal, B., 2005. Sea-ice extent and variability in the Nordic Seas, 1967—2002. In: Drange, H., Dokken, T., Furevik, T., Gerdes, R., Berger, W. (Eds.), The Nordic Seas: An Integrated Perspective. American Geophysical Union, Washington DC, pp. 39–49. http://dx.doi.org/10.1029/GM158.
Kwok, R., Cunningham, G.F., 2010. Contribution of melt in the Beaufort Sea to the decline in Arctic multiyear sea ice coverage: 1993–2009. Geophys. Res. Lett. 37, L20501. http://dx.doi.org/10.1029/2010GL044678.
Kwok, R., Cunningham, G.F., Pang, S.S., 2004. Fram Strait sea ice outflow. J. Geophys. Res. Oceans 109, C01009. http://dx.doi.org/10.1029/2003JC001785.
Lancelot, C., Hannon, E., Becquevort, S., Veth, C., De Baar, H.J.W., 2000. Modeling phytoplankton blooms and carbon export production in the Southern Ocean: dominant controls by light and iron in the Atlantic sector in Austral spring 1992. Deep-Sea Res. Part Oceanogr. Res. Pap. 47, 1621–1662. http://dx.doi.org/10.1016/S0967-0637(00)00005-4.
Lannuzel, D., Schoemann, V., de Jong, J., Pasquer, B., van der Merwe, P., Masson, F., Tison, J.-L., Bowie, A., 2010. Distribution of dissolved iron in Antarctic sea ice: spatial, seasonal, and inter-annual variability. J. Geophys. Res. Biogeosci. 115, G03022. http://dx.doi.org/10.1029/2009JG001031.
Lee, K., Kim, T.-W., Byrne, R.H., Millero, F.J., Feely, R.A., Liu, Y.-M., 2010. The universal ratio of boron to chlorinity for the North Pacific and North Atlantic oceans. Geochim. Cosmochim. Acta 74, 1801–1811. http://dx.doi.org/10.1016/j.gca.2009.12.027.
Lee, K., Millero, F.J., Byrne, R.H., Feely, R.A., Wanninkhof, R., 2000. The recommended dissociation constants for carbonic acid in seawater. Geophys. Res. Lett. 27, 229–232. http://dx.doi.org/10.1029/1999GL002345.
Le Moigne, F.A.C., Poulton, A.J., Henson, S.A., Daniels, C.J., Fragoso, G.M., Mitchell, E., Richier, S., Russell, B.C., Smith, H.E.K., Tarling, G.A., Young, J.R., Zubkov, M., 2015. Carbon export efficiency and phytoplankton community composition in the Atlantic sector of the Arctic Ocean. J. Geophys. Res. Oceans 120, 3896–3912. http://dx.doi.org/10.1002/2015JC010700.
Lewis, C.N., Brown, K.A., Edwards, L.A., Cooper, G., Findlay, H.S., 2013. Sensitivity to ocean acidification parallels natural pCO_2 gradients experienced by Arctic copepods under winter sea ice. Proc. Natl. Acad. Sci. 110, E4960–E4967. http://dx.doi.org/10.1073/pnas.1315162110.
Loeng, H., 1991. Features of the physical oceanographic conditions of the Barents Sea. Polar Res. 10, 5–18. http://dx.doi.org/10.1111/j.1751-8369.1991.tb00630.x.
Lueker, T.J., Dickson, A.G., Keeling, C.D., 2000. Ocean pCO_2 calculated from dissolved inorganic carbon, alkalinity, and equations for K1 and K2: validation based on laboratory measurements of CO_2 in gas and seawater at equilibrium. Mar. Chem. 70, 105–119. http://dx.doi.org/10.1016/S0304-4203(00)00022-0.
Maksym, T., Stammerjohn, S.E., Ackley, S., Massom, R., 2012. Antarctic Sea ice-a polar opposite? Oceanography 25, 140–151.
Marshall, J., Speer, K., 2012. Closure of the meridional overturning circulation through Southern Ocean upwelling. Nat. Geosci. 5, 171–180. http://dx.doi.org/10.1038/ngeo1391.
Martiny, A.C., Vrugt, J.A., Primeau, F.W., Lomas, M.W., 2013. Regional variation in the particulate organic carbon to nitrogen ratio in the surface ocean. Glob. Biogeochem. Cycles 27, 723–731. http://dx.doi.org/10.1002/gbc.20061.
Mathis, J.T., Cross, J.N., Bates, N.R., 2011. Coupling primary production and terrestrial runoff to ocean acidification and carbonate mineral suppression in the eastern Bering Sea. J. Geophys. Res.-Oceans 116, C02030. http://dx.doi.org/10.1029/2010jc006453.
Mattsdotter Björk, M., Fransson, A., Torstensson, A., Chierici, M., 2014. Ocean acidification state in western Antarctic surface waters: controls and interannual variability. Biogeosciences 11, 57–73. http://dx.doi.org/10.5194/bg-11-57-2014.
McNeil, B.I., Matear, R.J., 2008. Southern Ocean acidification: a tipping point at 450-ppm atmospheric CO_2. Proc. Natl. Acad. Sci. USA 105, 18860–18864. http://dx.doi.org/10.1073/pnas.0806318105.
Mehrbach, C., Culberson, C.H., Hawley, J.E., Pytkowicz, R.M., 1973. Measurement of the apparent dissociation constants of carbonic acid in seawater at atmospheric pressure. Limnol. Oceanogr. 18, 897–907. http://dx.doi.org/10.4319/lo.1973.18.6.0897.
Meredith, M.P., Watkins, J.L., Murphy, E.J., Cunningham, N.J., Wood, A.G., Korb, R., Whitehouse, M.J., Thorpe, S.E., Vivier, F., 2003. An anticyclonic circulation above the Northwest Georgia Rise, Southern Ocean. Geophys. Res. Lett. 30, 2061. http://dx.doi.org/10.1029/2003GL018039.
Miller, L.A., Chierici, M., Johannessen, T., Noji, T.T., Rey, F., Skjelvan, I., 1999. Seasonal dissolved inorganic carbon variations in the Greenland Sea and implications for atmospheric CO_2 exchange. Deep-Sea Res. Part II Top. Stud. Oceanogr. 46, 1473–1496. http://dx.doi.org/10.1016/S0967-0645(99)00031-4.
Milne, A., Landing, W., Bizimis, M., Morton, P., 2010. Determination of Mn, Fe, Co, Ni, Cu, Zn, Cd and Pb in seawater using high resolution magnetic sector inductively coupled mass spectrometry (HR-ICP-MS). Anal. Chim. Acta 665, 200–207. http://dx.doi.org/10.1016/j.aca.2010.03.027.
Nelson, D.M., Smith Jr., W.O., 1991. Sverdrup revisited: critical depths, maximum chlorophyll levels, and the control of Southern Ocean productivity by the irradiance-mixing regime. Limnol. Oceanogr. 36, 1650–1661. http://dx.doi.org/10.4319/lo.1991.36.8.1650.
Nielsdóttir, M.C., Bibby, T.S., Moore, C.M., Hinz, D.J., Sanders, R., Whitehouse, M., Korb, R., Achterberg, E.P., 2012. Seasonal and spatial dynamics of iron availability in the Scotia Sea. Mar. Chem. 130–131, 62–72. http://dx.doi.org/10.1016/j.marchem.2011.12.004.
Nowlin, W.D., Klinck, J.M., 1986. The physics of the Antarctic Circumpolar Current. Rev. Geophys. 24, 469–491. http://dx.doi.org/10.1029/RG024i003p00469.
Orr, J.C., Fabry, V.J., Aumont, O., Bopp, L., Doney, S.C., Feely, R.A., Gnanadesikan, A., Gruber, N., Ishida, A., Joos, F., Key, R.M., Lindsay, K., Maier-Reimer, E., Matear, R., Monfray, P., Mouchet, A., Najjar, R.G., Plattner, G.-K., Rodgers, K.B., Sabine, C.L., Sarmiento, J.L., Schlitzer, R., Slater, R.D., Totterdell, I.J., Weirig, M.-F., Yamanaka, Y., Yool, A., 2005. Anthropogenic ocean acidification over the twenty-first century and its impact on calcifying organisms. Nature 437, 681–686. http://dx.doi.org/10.1038/nature04095.
Orsi, A.H., Whitworth III, T., Nowlin Jr., W.D., 1995. On the meridional extent and fronts of the Antarctic Circumpolar Current. Deep-Sea Res. Part Oceanogr. Res. Pap. 42, 641–673. http://dx.doi.org/10.1016/0967-0637(95)00021-W.
Park, J., Oh, I.-S., Kim, H.-C., Yoo, S., 2010. Variability of SeaWiFs chlorophyll-a in the southwest Atlantic sector of the Southern Ocean: strong topographic effects and weak seasonality. Deep-Sea Res. Part Oceanogr. Res. Pap. 57, 604–620. http://dx.doi.org/10.1016/j.dsr.2010.01.004.
Peck, V.L., Tarling, G.A., Manno, C., Harper, E.M., Tynan, E., 2016. Outer organic layer and internal repair mechanism protects pteropod *Limacina helicina* from ocean acidification. Deep Sea Res. Part II: Top. Stud. Oceanogr. Available online 15.12.15. 127, 57–59. 〈http://dx.doi.org/10.1016/j.dsr2.2015.12.005〉.
Poulton, A.J., Daniels, C.J., Esposito, M., Humphreys, M.P., Mitchell, E., Ribas-Ribas, M., Russell, B.C., Stinchcombe, M.C., Tynan, E., Richier, S., 2016. Production of dissolved organic carbon by Arctic plankton communities: responses to elevated carbon dioxide and the availability of light and nutrients. Deep Sea Res. Part II: Top. Stud. Oceanogr. Available online 14.01.16. 127, 60–74. 〈http://dx.doi.org/10.1016/j.dsr2.2016.01.002〉.

Quay, P., Sonnerup, R., Westby, T., Stutsman, J., McNichol, A., 2003. Changes in the 13C/12C of dissolved inorganic carbon in the ocean as a tracer of anthropogenic CO_2 uptake. Glob. Biogeochem. Cycles 17, 1004. http://dx.doi.org/10.1029/2001GB001817.

Rees, A.P., Brown, I.J., Jayakumar, A., Ward, B.B., 2016. The inhibition of N_2O production by ocean acidification in cold temperate and polar waters. Deep Sea Res. Part II: Top. Stud. Oceanogr. Available online 17.12.15. 127, 93–101. 〈http://dx.doi.org/10.1016/j.dsr2.2015.12.006〉.

Reid, P., Stammerjohn, S., Massom, R., Scambos, T., Felden, J., 2015. The record 2013 Southern Hemisphere sea-ice extent maximum. Ann. Glaciol. 56, 99–106. http://dx.doi.org/10.3189/2015AoG69A892.

Rérolle, V.M.C., Floquet, C.F.A., Harris, A.J.K., Mowlem, M.C., Bellerby, R.G.J., Achterberg, E.P., 2013. Development of a colorimetric microfluidic pH sensor for autonomous seawater measurements. Anal. Chim. Acta 786, 124–131. http://dx.doi.org/10.1016/j.aca.2013.05.008.

Rérolle, V.M.C., Floquet, C.F.A., Mowlem, M.C., Connelly, D.P., Achterberg, E.P., Bellerby, R.R.G.J., 2012. Seawater-pH measurements for ocean-acidification observations. TrAC Trends Anal. Chem. 40, 146–157. http://dx.doi.org/10.1016/j.trac.2012.07.016.

Ribas-Ribas, M., Rérolle, V.M.C., Bakker, D.C.E., Kitidis, V., Lee, G.A., Brown, I., Achterberg, E.P., Hardman-Mountford, N.J., Tyrrell, T., 2014. Intercomparison of carbonate chemistry measurements on a cruise in northwestern European shelf seas. Biogeosciences 11, 4339–4355. http://dx.doi.org/10.5194/bg-11-4339-2014.

Ries, J.B., Cohen, A.L., McCorkle, D.C., 2009. Marine calcifiers exhibit mixed responses to CO_2-induced ocean acidification. Geology 37, 1131–1134. http://dx.doi.org/10.1130/G30210A.1.

Rio, M.-H., Hernandez, F., 2004. A mean dynamic topography computed over the world ocean from altimetry, in situ measurements, and a geoid model. J. Geophys. Res. Oceans 109, C12032. http://dx.doi.org/10.1029/2003JC002226.

Robbins, L.L., Wynn, J.G., Lisle, J.T., Yates, K.K., Knorr, P.O., Byrne, R.H., Liu, X., Patsavas, M.C., Azetsu-Scott, K., Takahashi, T., 2013. Baseline monitoring of the western arctic ocean estimates 20% of Canadian basin surface waters are undersaturated with respect to Aragonite. Plos One 8, e73796. http://dx.doi.org/10.1371/journal.pone.0073796.

Roden, N.P., Shadwick, E.H., Tilbrook, B., Trull, T.W., 2013. Annual cycle of carbonate chemistry and decadal change in coastal Prydz Bay, East Antarctica. Mar. Chem. 155, 135–147. http://dx.doi.org/10.1016/j.marchem.2013.06.006.

Roy, R.N., Roy, L.N., Vogel, K.M., Porter-Moore, C., Pearson, T., Good, C.E., Millero, F.J., Campbell, D.M., 1993. The dissociation constants of carbonic acid in seawater at salinities 5 to 45 and temperatures 0 to 45 °C. Mar. Chem. 44, 249–267. http://dx.doi.org/10.1016/0304-4203(93)90207-5.

Rudels, B., Björk, G., Nilsson, J., Winsor, P., Lake, I., Nohr, C., 2005. The interaction between waters from the Arctic Ocean and the Nordic Seas north of Fram Strait and along the East Greenland Current: results from the Arctic Ocean-02 Oden expedition. J. Mar. Syst. 55, 1–30. http://dx.doi.org/10.1016/j.jmarsys.2004.06.008.

Rysgaard, S., Bendtsen, J., Pedersen, L.T., Ramlov, H., Glud, R.N., Ramløv, H., 2009. Increased CO_2 uptake due to sea ice growth and decay in the Nordic Seas. J Geophys Res 114, C09011. http://dx.doi.org/10.1029/2008jc005088.

Sabine, C.L., Feely, R.A., Gruber, N., Key, R.M., Lee, K., Bullister, J.L., Wanninkhof, R., Wong, C.S., Wallace, D.W.R., Tilbrook, B., Millero, F.J., Peng, T.-H., Kozyr, A., Ono, T., Rios, A.F., 2004. The oceanic sink for anthropogenic CO_2. Science 305, 367–371. http://dx.doi.org/10.1126/science.1097403.

Sakshaug, E., 2004. Primary and secondary production in the Arctic Seas. In: Stein, R., Macdonald, R. (Eds.), The Organic Carbon Cycle in the Arctic Ocean. Springer, pp. 57–81, 10.1007/978-3-642-18912-8, Berlin.

Sambrotto, R.N., Savidge, G., Robinson, C., Boyd, P., Takahashi, T., Karl, D.M., Langdon, C., Chipman, D., Marra, J., Codispoti, L., 1993. Elevated consumption of carbon relative to nitrogen in the surface ocean. Nature 363, 248–250. http://dx.doi.org/10.1038/363248a0.

Savidge, G., Priddle, J., Gilpin, L.C., Bathmann, U., Murphy, E.J., Owens, N.J.P., Pollard, R.T., Turner, D.R., Veth, C., Boyd, P., 1996. An assessment of the role of the marginal ice zone in the carbon cycle of the Southern Ocean. Antarct. Sci. 8, 349–358. http://dx.doi.org/10.1017/S0954102096000521.

Schlitzer, R., 2002. Carbon export fluxes in the Southern Ocean: results from inverse modeling and comparison with satellite-based estimates. Deep-Sea Res. Part II Top. Stud. Oceanogr. 49, 1623–1644. http://dx.doi.org/10.1016/S0967-0645(02)00004-8.

Schmidtko, S., Johnson, G.C., Lyman, J.M., 2013. MIMOC: a global monthly isopycnal upper-ocean climatology with mixed layers. J. Geophys. Res. Oceans 118, 1658–1672. http://dx.doi.org/10.1002/jgrc.20122.

Serreze, M.C., Barrett, A.P., Stroeve, J.C., Kindig, D.N., Holland, M.M., 2009. The emergence of surface-based Arctic amplification. Cryosphere 3, 11–19. http://dx.doi.org/10.5194/tc-3-11-2009.

Shadwick, E.H., Rintoul, S.R., Tilbrook, B., Williams, G.D., Young, N., Fraser, A.D., Marchant, H., Smith, J., Tamura, T., 2013a. Glacier tongue calving reduced dense water formation and enhanced carbon uptake. Geophys. Res. Lett. 40, 904–909. http://dx.doi.org/10.1002/grl.50178.

Shadwick, E.H., Trull, T.W., Thomas, H., Gibson, J.A.E., 2013b. Vulnerability of Polar Oceans to anthropogenic acidification: comparison of Arctic and Antarctic seasonal cycles. Sci Rep 3, 2339. http://dx.doi.org/10.1038/srep02339.

Shapiro, I., Colony, R., Vinje, T., 2003. April sea ice extent in the Barents Sea, 1850–2001. Polar Res. 22, 5–10. http://dx.doi.org/10.1111/j.1751-8369.2003.tb00089.x.

Skjelvan, I., Falck, E., Rey, F., Kringstad, S.B., 2008. Inorganic carbon time series at Ocean Weather Station M in the Norwegian Sea. Biogeosciences 5, 549–560. http://dx.doi.org/10.5194/bg-5-549-2008.

Skjelvan, I., Johannessen, T., Miller, L.A., 1999. Interannual variability of fCO_2 in the Greenland and Norwegian Seas. Tellus B 51, 477–489. http://dx.doi.org/10.1034/j.1600-0889.1999.00024.x.

Skogen, M.D., Olsen, A., Børsheim, K.Y., Sandø, A.B., Skjelvan, I., 2014. Modelling ocean acidification in the Nordic and Barents Seas in present and future climate. J. Mar. Syst 131, 10–20. http://dx.doi.org/10.1016/j.jmarsys.2013.10.005.

Skoog, A., Lara, R., Kattner, G., 2001. Spring–summer cycling of DOC, DON and inorganic N in a highly seasonal system encompassing the Northeast Water Polynya, 1993. Deep-Sea Res. Part Oceanogr. Res. Pap. 48, 2613–2629. http://dx.doi.org/10.1016/S0967-0637(01)00029-2.

Stammerjohn, S.E., Martinson, D.G., Smith, R.C., Yuan, X., Rind, D., 2008. Trends in Antarctic annual sea ice retreat and advance and their relation to El Niño–Southern Oscillation and Southern Annular Mode variability. J. Geophys. Res. 113. http://dx.doi.org/10.1029/2007JC004269.

Steinacher, M., Joos, F., Frölicher, T.L., Plattner, G.-K., Doney, S.C., 2009. Imminent ocean acidification in the Arctic projected with the NCAR global coupled carbon cycle-climate model. Biogeosciences 6, 515–533. http://dx.doi.org/10.5194/bg-6-515-2009.

Stocker, T.F., Qin, D., Plattner, G.-K., Tignor, M., Allen, S.K., Boschung, J., Nauels, A., Xia, Y., Bex, V., Midgley, P.M., 2013. IPCC, 2013: Climate Change 2013: The Physical Science Basis. IPCC. Cambridge University Press, Cambridge, United Kingdom.

Stroeve, J.C., Serreze, M.C., Fetterer, F., Arbetter, T., Meier, W., Maslanik, J., Knowles, K., 2005. Tracking the Arctic's shrinking ice cover: another extreme September minimum in 2004. Geophys. Res. Lett. 32, L04501. http://dx.doi.org/10.1029/2004GL021810.

Stroeve, J.C., Serreze, M.C., Holland, M.M., Kay, J.E., Malanik, J., Barrett, A.P., 2012. The Arctic's rapidly shrinking sea ice cover: a research synthesis. Clim. Change 110, 1005–1027. http://dx.doi.org/10.1007/S10584-011-0101-1.

Strong, C., Rigor, I.G., 2013. Arctic marginal ice zone trending wider in summer and narrower in winter. Geophys. Res. Lett. 40, 4864–4868. http://dx.doi.org/10.1002/grl.50928.

Svendsen, H., Beszczynska-Møller, A., Hagen, J.O., Lefauconnier, B., Tverberg, V., Gerland, S., Ørbøk, J.B., Bischof, K., Papucci, C., Zajaczkowski, M., Azzolini, R., Bruland, O., Wiencke, C., Winther, J.-G., Dallmann, W., 2002. The physical environment of Kongsfjorden–Krossfjorden, an Arctic fjord system in Svalbard. Polar Res. 21, 133–166. http://dx.doi.org/10.1111/j.1751-8369.2002.tb00072.x.

Swift, J.H., Aagaard, K., 1981. Seasonal transitions and water mass formation in the Iceland and Greenland seas. Deep-Sea Res. Part Oceanogr. Res. Pap. 28, 1107–1129. http://dx.doi.org/10.1016/0198-0149(81)90050-9.

Tagliabue, A., Sallée, J.-B., Bowie, A.R., Lévy, M., Swart, S., Boyd, P.W., 2014. Surface-water iron supplies in the Southern Ocean sustained by deep winter mixing. Nat. Geosci. 7, 314–320. http://dx.doi.org/10.1038/ngeo2101.

Takahashi, T., Sutherland, S.C., Wanninkhof, R., Sweeney, C., Feely, R.A., Chipman, D. W., Hales, B., Friederich, G., Chavez, F., Sabine, C., Watson, A., Bakker, D.C.E., Schuster, U., Metzl, N., Yoshikawa-Inoue, H., Ishii, M., Midorikawa, T., Nojiri, Y., Körtzinger, A., Steinhoff, T., Hoppema, M., Olafsson, J., Arnarson, T.S., Tilbrook, B., Johannessen, T., Olsen, A., Bellerby, R., Wong, C.S., Delille, B., Bates, N.R., de Baar, H.J.W., 2009. Climatological mean and decadal change in surface ocean pCO_2, and net sea–air CO_2 flux over the global oceans. Deep-Sea Res. Part II Top. Stud. Oceanogr. 56, 554–577. http://dx.doi.org/10.1016/j.dsr2.2008.12.009.

Takeda, S., 1998. Influence of iron availability on nutrient consumption ratio of diatoms in oceanic waters. Nature 393, 774–777. http://dx.doi.org/10.1038/31674.

Thompson, M., Howarth, R.J., 1973. The rapid estimation and control of precision by duplicate determinations. Analyst 98, 153–160. http://dx.doi.org/10.1039/AN9739800153.

Turner, J., Overland, J., 2009. Contrasting climate change in the two polar regions. Polar Res. 28, 146–164. http://dx.doi.org/10.3402/polar.v28i2.6120.

Tynan, E., Tyrrell, T., Achterberg, E.P., 2014. Controls on the seasonal variability of calcium carbonate saturation states in the Atlantic gateway to the Arctic Ocean. Mar. Chem. 158, 1–9. http://dx.doi.org/10.1016/j.marchem.2013.10.010.

Van Heuven, S.M.A.C., Hoppema, M., Huhn, O., Slagter, H.A., de Baar, H.J.W., 2011a. Direct observation of increasing CO_2 in the Weddell Gyre along the Prime Meridian during 1973–2008. Deep-Sea Res. Part II Top. Stud. Oceanogr. 58, 2613–2635. http://dx.doi.org/10.1016/j.dsr2.2011.08.007.

Van Heuven, S., Pierrot, D., Rae, J.W.B., Lewis, E., Wallace, D.W.R., 2011b. MATLAB Program Developed for CO_2 System Calculations, ORNL/CDIAC-105b. Oak Ridge National Laboratory, U.S. Department of Energy, Oak Ridge, Tennessee, Carbon Dioxide Information Analysis Center.

Vaughan, D.G., Marshall, G.J., Connolley, W.M., Parkinson, C., Mulvaney, R., Hodgson, D.A., King, J.C., Pudsey, C.J., Turner, J., 2003. Recent rapid regional climate warming on the Antarctic Peninsula. Clim. Change 60, 243–274. http://dx.doi.org/10.1023/A:1026021217991.

Venables, H., Meredith, M.P., Atkinson, A., Ward, P., 2012. Fronts and habitat zones in the Scotia Sea. Deep-Sea Res. Part II Top. Stud. Oceanogr. 59–60, 14–24. http://dx.doi.org/10.1016/j.dsr2.2011.08.012.

Vinje, T., 2001. Anomalies and trends of sea-ice extent and atmospheric circulation in the Nordic Seas during the Period 1864–1998. J. Clim. 14, 255–267. http://dx.doi.org/10.1175/1520-0442(2001)014 < 0255:AATOSI > 2.0.CO;2.

Whitworth, T., Nowlin Jr, W.D., Orsi, A.H., Locarnini, R.A., Smith, S.G., 1994. Weddell Sea shelf water in the Bransfield Strait and Weddell-Scotia Confluence. Deep-Sea Res. Part Oceanogr. Res. Pap. 41, 629–641. http://dx.doi.org/10.1016/0967-0637(94)90046-9.

Wolf-Gladrow, D.A., Zeebe, R.E., Klaas, C., Kortzinger, A., Dickson, A.G., 2007. Total alkalinity: the explicit conservative expression and its application to biogeochemical processes. Mar. Chem. 106, 287–300. http://dx.doi.org/10.1016/j.marchem.2007.01.006.

Woodgate, R.A., Fahrbach, E., Rohardt, G., 1999. Structure and transports of the East Greenland Current at 75°N from moored current meters. J. Geophys. Res. Oceans 104, 18059–18072. http://dx.doi.org/10.1029/1999JC900146.

Wouters, B., Martin-Español, A., Helm, V., Flament, T., Wessem, J.M., van, Ligtenberg, S.R.M., Broeke, M.R., van den, Bamber, J.L., 2015. Dynamic thinning of glaciers on the Southern Antarctic Peninsula. Science 348, 899–903. http://dx.doi.org/10.1126/science.aaa5727.

Yager, P.L., Wallace, D.W.R., Johnson, K.M., Smith, W.O., Minnett, P.J., Deming, J.W., 1995. The Northeast Water Polynya as an atmospheric CO_2 sink: a seasonal rectification hypothesis. J. Geophys. Res. Oceans 100, 4389–4398. http://dx.doi.org/10.1029/94JC01962.

Yamamoto-Kawai, M., McLaughlin, F.A., Carmack, E.C., Nishino, S., Shimada, K., 2009. Aragonite undersaturation in the Arctic Ocean: effects of ocean acidification and sea ice melt. Science 326, 1098–1100. http://dx.doi.org/10.1126/science.1174190.

Zeebe, R.E., Wolf-Gladrow, D., 2001. CO_2 in Seawater: Equilibrium, Kinetics, Isotopes. Elsevier, Amsterdam.

Zhang, H., Byrne, R.H., 1996. Spectrophotometric pH measurements of surface seawater at in-situ conditions: absorbance and protonation behavior of thymol blue. Mar. Chem. 52, 17–25. http://dx.doi.org/10.1016/0304-4203(95)00076-3.

Zhou, J., Delille, B., Eicken, H., Vancoppenolle, M., Brabant, F., Carnat, G., Geilfus, N.-X., Papakyriakou, T., Heinesch, B., Tison, J.-L., 2013. Physical and biogeochemical properties in landfast sea ice (Barrow, Alaska): insights on brine and gas dynamics across seasons. J. Geophys. Res. Oceans 118, 3172–3189. http://dx.doi.org/10.1002/jgrc.20232.

Ziveri, P., Rutten, A., de Lange, D.J., Thomson, J., Corselli, C., 2000. Present-day coccolith fluxes recorded in central eastern Mediterranean sediment traps and surface sediments. Palaeogeogr. Palaeoclimatol. Palaeoecol. 158, 175–195. http://dx.doi.org/10.1016/S0031-0182(00)00049-3.